Intestine-enriched *apolipoprotein b* orthologs are required for stem cell differentiation and regeneration in planarians

Lily L. Wong[1,*], Christina G. Bruxvoort[1,2,*], Nicholas I. Cejda[1], Jannette Rodriguez Otero[3,4], and David J. Forsthoefel[1,5,#]

[1] Genes and Human Disease Research Program, Oklahoma Medical Research Foundation, Oklahoma City, Oklahoma

[2] Current address: Arthritis and Clinical Immunology Research Program, Oklahoma Medical Research Foundation; Department of Pathology, University of Oklahoma Health Sciences Center; and Department of Veteran Affairs Medical Center - Research Services, Oklahoma City, Oklahoma

[3] Howard Hughes Medical Institute, Department of Cell and Developmental Biology, University of Illinois at Urbana-Champaign, Urbana, Illinois

[4] Current address: Department of Education, Universidad Interamericana de Puerto Rico, San Juan, Puerto Rico

[5] Department of Cell Biology, University of Oklahoma Health Sciences Center, Oklahoma City, Oklahoma

* Authors contributed equally

[#] Correspondence:

David J. Forsthoefel, Ph.D.: david-forsthoefel@omrf.org

Abstract

Lipid metabolism plays an instructive role in regulating stem cell state and differentiation. However, the roles of lipid mobilization and utilization in stem cell-driven regeneration are unclear. Planarian flatworms readily restore missing tissue due to injury-induced activation of pluripotent somatic stem cells called neoblasts. Here, we identify two intestine-enriched orthologs of *apolipoprotein b, apob-1* and *apob-2,* which mediate transport of neutral lipid stores from the intestine to target tissues including neoblasts, and are required for tissue homeostasis and regeneration. Inhibition of *apob* function by RNAi causes head regression and lysis in uninjured animals, and delays body axis re-establishment and regeneration of multiple organs in amputated fragments. Furthermore, *apob* RNAi causes expansion of the population of differentiating neoblast progeny and dysregulates expression of genes enriched in differentiating and mature cells in eight major cell type lineages. We conclude that intestine-derived lipids serve as a source of metabolites required for neoblast differentiation.

41 ## Introduction

42 Regeneration requires metabolites and energy for cell proliferation, differentiation,
43 migration, and growth. Currently, specific mechanisms by which various metabolites are
44 produced, transported, and utilized to promote regeneration are not well understood. In animals,
45 neutral lipids (NLs) (e.g., triglycerides and cholesteryl esters) are stored in intracellular lipid
46 droplets, which serve as central organelles for energy and lipid homeostasis[1,2]. Lipid stores can
47 be mobilized either by NL packaging and export in lipoprotein particles (LPs), or by lipolysis and
48 secretion as fatty acids (FAs)[3-5]. Mobilization enables transport to other tissues, for example
49 between intestine, liver, and peripheral tissues such as brain and muscle in vertebrates, or
50 between the fat body, intestine, nervous system, and imaginal discs in *Drosophila*[6-8]. Upon
51 lipase-mediated hydrolysis of NLs, the FAs and cholesterol produced serve as building blocks
52 for membrane biosynthesis, substrates for energy via fatty acid beta oxidation, sources of
53 acetyl-CoA and other precursors for chromatin remodeling, and precursors of signaling
54 molecules like eicosanoids and sphingolipids[9-11].

55 Considerable evidence indicates that disruption of lipid catabolism, biosynthesis, and
56 transport can dysregulate stem cell pluripotency, proliferation, and differentiation[12-14]. For
57 example, inhibiting fatty acid oxidation (FAO, the process of converting fatty acids to acetyl-
58 CoA) causes symmetric production of differentiating progeny and stem cell depletion in the
59 mammalian hematopoietic lineage[15]. By contrast, in the adult mouse hippocampus, inhibiting
60 FAO promotes exit from quiescence and proliferation of neural stem/progenitor cells in the adult
61 mouse hippocampus[16]. In *Drosophila*, compromising lipolysis and/or FAO causes intestinal stem
62 cell necrosis[17], and loss of germline stem cells[18]. On the other hand, FAO-mediated production
63 of acetyl-CoA (a precursor for histone acetylation) is required for differentiation, but not
64 maintenance, of quiescent hematopoietic stem cells in *Drosophila* larvae, illustrating the growing
65 recognition of the intersection of lipid metabolism and epigenetic regulation[19]. Perturbing lipid

66 synthesis and delivery also dysregulates stem cell state and differentiation dynamics. For
67 example, inhibiting fatty acid synthase (required for *de novo* lipogenesis) reduces proliferation
68 by adult mouse neural stem and progenitor cells[20]. Similarly, mutations in *hydroxysteroid (17-*
69 *beta) dehydrogenase 7*, a regulator of cholesterol biosynthesis, cause premature differentiation
70 of neural progenitors during development[21]. In culture, depriving human pluripotent stem cells of
71 extrinsic lipids promotes a "naive-to-primed" intermediate state, demonstrating the importance
72 of exogenous lipid availability for regulation of stem cell state[22].

73 Because stem and progenitor cell activation, proliferation, and differentiation are central
74 to regeneration, these diverse observations underline the potential importance of lipid
75 metabolism during regenerative growth. Currently, however, evidence that lipid transport and
76 utilization influence regeneration is limited. In zebrafish, *leptin b* (a hormonal regulator of
77 systemic lipid metabolism) is one of the most upregulated genes during fin and heart
78 regeneration[23], and *apolipoprotein E* (a regulator of NL transport in LPs) is upregulated during
79 fin regeneration[24]. In the axolotl *Ambystoma mexicanum*, genes involved in steroid, cholesterol,
80 and fatty acid metabolism are among the most upregulated at later stages of limb regeneration,
81 when differentiation of cartilage and muscle progenitors occurs[25]. In a primary cell culture model
82 of nerve injury, rat retinal ganglion cells regrow projections after axotomy more efficiently in the
83 presence of glial-derived LPs, reinforcing the role of cholesterol in axon regeneration[26]. In mice,
84 *low density lipoprotein receptor* deficiency delays liver regeneration and reduces hepatocyte
85 proliferation[27]. Similarly, elevated FA levels (induced by lipoprotein lipase overexpression)
86 causes lipotoxicity and compromises skeletal muscle regeneration[28], while inhibition of
87 peroxisomal FAO induces differentiation of myogenic satellite cells and muscle hypertrophy
88 during regeneration[29]. During skin wound repair, inhibiting triglyceride lipase-mediated lipolysis
89 by dermal adipocytes compromises recruitment of inflammatory macrophages and adipocyte
90 fate-switching to extracellular-matrix-secreting myofibroblasts[30].

91 Although these intriguing observations point to the importance of lipid metabolism, there
92 is scant functional understanding of how lipid transport and utilization influence stem cell
93 regulation during regeneration, particularly in emerging animal models with extensive
94 regenerative capacity. Planarians are freshwater flatworms capable of whole-body regeneration,
95 an ability conferred by pluripotent somatic stem cells called neoblasts that divide and
96 differentiate to replace damaged and lost tissues after amputation[31,32]. Diet-derived NLs are
97 stored in the planarian intestine in lipid droplets, suggesting the intestine is a major lipid storage
98 organ, as in *Drosophila* and *C. elegans*[6,33-35]. Planarian intestinal lipids have been proposed to
99 be a source of metabolites during extended fasting, as well as regeneration[34,36,37]. However,
100 mechanisms by which lipid secretion is controlled, and whether delivery to neoblasts or their
101 progeny is functionally required for regeneration, have not been investigated.
102 In this study, we show that two intestine-enriched *apolipoprotein b* (*apob*) orthologs are
103 required for NL transport from the intestine to neoblasts and their progeny, and that ApoB
104 function is required for stem cell differentiation and regeneration in the planarian *Schmidtea*
105 *mediterranea*. In mammals and insects, ApoB and ApoB-like proteins mediate trafficking of NLs
106 in LPs from digestive and storage organs to peripheral target tissues[5,38]. Here, we identify adult
107 stem cells and their differentiating progeny as additional target tissues for ApoB-mediated NL
108 transport in a regeneration competent animal, and propose utilizing planarians as models to
109 understand the influence of lipid metabolism on stem cells during regeneration.
110

111 ## Results

112 **Planarian *apolipoprotein b* orthologs are expressed by intestinal cells**

113 Previously, we demonstrated that knockdown of an intestine-enriched transcription
114 factor, *nkx2.2*, inhibited neoblast proliferation and formation of the regeneration blastema, the
115 unpigmented mass of tissue produced after amputation[39]. These observations suggested that
116 the intestine could play a non-autonomous role in regulating stem cell dynamics. In an effort to
117 identify intestine-enriched transcripts encoding neoblast regulators, we generated
118 transcriptomes from control and *nkx2.2(RNAi)* planarians, in which neoblast proliferation and
119 regenerative tissue production are severely inhibited (Supplementary Fig. 1a-c)[39]. An ortholog of
120 human *apolipoprotein b* ("*apob-1*") encoding conserved Vitellogenin, DUF1943, and von
121 Willebrand Factor D domains, was the second-most-downregulated transcript by significance
122 and fold-change, while a paralog, *apob-2,* was also significantly downregulated (Fig. 1a;
123 Supplementary Fig. 1d, e; Supplementary Data 1a-c; and Supplementary Data 2a-b).
124 Consistent with single cell expression profiling[40] (Supplementary Fig. 1f), both transcripts were
125 highly enriched in intestinal phagocytes, absorptive cells responsible for digestion, nutrient
126 storage, and metabolite secretion (Fig. 1b and Supplementary Fig. 1f, g). In addition, both
127 transcripts were weakly expressed in a small number of cells outside the intestine likely to be
128 differentiating neoblast progeny (Fig. 1b and Supplementary Fig. 1f).
129

130 **ApoB orthologs are required for viability and regulate neutral lipid transport**

131 To determine whether ApoB orthologs were required for homeostatic tissue renewal
132 and/or regeneration, we knocked down *apob-1* and *apob-2* using RNA interference[41]. In
133 uninjured planarians, knockdown of either *apob-1* or *apob-2* individually had no phenotype (not
134 shown), suggesting functional redundancy. However, after 3-5 double-stranded RNA (dsRNA)
135 feedings, double knockdown *apob(RNAi)* animals displayed phenotypes that progressed from

136 mild (modest/regional pigmentation loss), to severe (animal-wide pigmentation loss and reduced
137 motility), to very severe (head regression, ventral curling, and eventual lysis) (Fig. 2a). Head
138 regression and ventral curling phenotypes are common in planarians lacking functional
139 neoblasts[42], and suggested that ApoB orthologs could have functional roles in the regulation of
140 planarian stem cells.

141 ApoB orthologs in vertebrates and insects regulate LP biogenesis and secretion[5,43]. To
142 test whether ApoB protein was secreted, we made a custom antibody recognizing the N-
143 terminus of Smed-ApoB-1 (Fig. 2b, c). ApoB-1 protein was enriched in the intestine, but also
144 throughout the parenchyma (tissues surrounding other organs, sandwiched between the
145 epidermis and intestine, where neoblasts also reside). This indicated that although *apob*
146 mRNAs were intestine-enriched (Fig. 1a, b), ApoB protein was robustly secreted and
147 transported to peripheral tissues (Fig. 2c). Expression was dramatically reduced in both regions
148 in *apob-1;apob-2(RNAi)* double knockdown planarians (*"apob(RNAi)"* hereafter for brevity),
149 demonstrating that knockdown effectively reduced ApoB protein levels (Fig. 2c).

150 ApoB orthologs facilitate NL secretion and transport via LPs[5,38], while ApoB binding by
151 receptors mediate NL uptake and metabolism by target cells[44]. To test whether planarian ApoB
152 functioned similarly, we first evaluated NL distribution in *apob(RNAi)* animals. In histological
153 sections, NLs (labeled with Oil Red O) were elevated in both the intestine as well as tissues
154 surrounding the intestine, suggesting that both LP secretion by the intestine and
155 uptake/metabolism by peripheral tissues were compromised (Fig. 2d). Using thin layer
156 chromatography, we also found significant elevation of cholesteryl esters and triglycerides in
157 lipid extracts from *apob(RNAi)* animals (Fig. 2e). These phenotypes predicted that delivery of
158 NLs to neoblasts and/or their progeny would be compromised by ApoB inhibition. To test this,
159 we quantified NL content in neoblasts and their progeny using a fluorescent NL probe, BODIPY-
160 493/503, by flow cytometry. Three major subpopulations of planarian cells can be distinguished
161 by their DNA content and sensitivity to X-irradiation[45,46] (Fig. 2f-h). The "X1" fraction/gate

162 includes >2C DNA content neoblasts in S/G2/M phase of the cell cycle, while "X2" includes 2C
163 neoblasts in G0/G1 and G0 post-mitotic progeny. "Xins," named for the fact that cells in this
164 gate are insensitive to X-irradiation, consists of later stage progeny and mature differentiated
165 cells. We found a dramatic reduction of fluorescence in both the X1 and X2 fractions in
166 *apob(RNAi)* animals vs. controls (Fig. 2i, j), indicating that a reduction of NL content in neoblasts
167 and their progeny was caused by ApoB inhibition. Together, these data demonstrated that
168 planarian ApoB proteins were produced by the intestine and were likely secreted as LPs to
169 transport NLs from the intestine to stem cells and their differentiating progeny.
170

171 ***apob* and *lipoprotein receptor* genes are upregulated in regenerating fragments**

172 Amputation induces changes in gene expression during planarian regeneration[47-49]. We
173 predicted that if *apob* and other genes involved in neutral lipid metabolism played functional
174 roles during regeneration, they would be up- or down-regulated in amputated tissue fragments.
175 Using quantitative PCR, we found that both *apob-1* and *apob-2* transcripts were upregulated in
176 tissue fragments at two distinct time points during earlier stages of regeneration commonly
177 associated with neoblast proliferation (1-3 days) and differentiation (4-5 days) (Supplementary
178 Fig. 2a, b). Upregulation of *apob-1* and *apob-2* was also observed in previously published RNA-
179 Seq data from a 14-day time course of whole-body planarian regeneration (Supplementary Fig.
180 2c)[49]. Using quantitative capillary-based Western blotting, we also found that ApoB-1 protein
181 levels increased by 3-5 days after amputation (Supplementary Fig. 2d). Consistently,
182 accumulation of neutral lipids was sustained in 3- and 6-day *apob(RNAi)* regenerates
183 (Supplementary Fig. 2e, f), suggesting that LP trafficking from the intestine was disrupted, as in
184 uninjured animals (Fig. 2d).

185 In addition, we found that three planarian orthologs of human lipoprotein receptors
186 (which bind apolipoproteins, enabling LP uptake/metabolism) were upregulated in the blastema,
187 and regenerating brain and pharynx (Supplementary Fig. 3a, b, d). These transcripts were

188 expressed in both *piwi-1*-mRNA-positive neoblasts as well as *piwi-1*-negative cells that were
189 likely to be differentiating neoblast progeny in the regenerating pharynx and blastema
190 (Supplementary Fig. 3d). Two lipoprotein receptor genes (*ldlr-1* and *ldlr-2*) were also
191 differentially expressed in the whole-body regeneration RNA-Seq dataset (Supplementary Fig.
192 3c)[49]. Using the Gene Ontology to mine the same dataset[49], we identified additional planarian
193 genes predicted to regulate lipid transport, triglyceride, and cholesterol metabolism, and found
194 that many of these transcripts were also up- and down-regulated during regeneration
195 (Supplementary Fig. 3e and Supplementary Data 3). Together, these observations indicate that
196 *apob-1, apob-2,* and other genes involved in neutral lipid metabolism were differentially
197 expressed in response to amputation, consistent with roles during regeneration.
198

199 ***apob* paralogs are required for polarity re-establishment and organogenesis during**
200 **regeneration**

201 To assess functional roles of *apob* paralogs during regeneration (Fig. 3a), we chose
202 uninjured animals after three dsRNA feedings that exhibited "mild" and "severe" phenotypes
203 (Fig. 2a), amputated their heads, and assessed blastema morphogenesis, which absolutely
204 requires neoblast proliferation and differentiation[50-52]. Controls, *apob-1(RNAi)*-only, and *apob-*
205 *2(RNAi)*-only fragments regenerated normally (Fig. 3b), again suggesting *apob* paralogs likely
206 functioned redundantly. However, *apob(RNAi)* double knockdown animals had reduced
207 posterior blastemas (head fragments) and anterior blastemas (trunk fragments) at 8 days post-
208 amputation (Fig. 3b). Blastema size was noticeably smaller in fragments from "severe" ("*apob-*
209 *S"*) animals compared to "mild" ("*apob-M"*) animals (Fig. 3b), suggesting that neoblasts and/or
210 their progeny were more strongly affected over time.

211 Expression of so-called "position control genes" to re-establish axial polarity is an
212 essential early event required for whole-body regeneration[53]. We asked whether expression of
213 anterior (*notum*)[54] or posterior (*wnt11-2*)[55] was affected in *apob(RNAi)* regenerates. Indeed, at

214 three days post-amputation (3 dpa), the number of both posterior *wnt11-2*-expressing cells (Fig.
215 3c) and anterior *notum*-expressing cells (Fig. 3d) was reduced in *apob-M* and *apob-S*
216 fragments. By 6 dpa, although most *apob(RNAi)* fragments had regenerated more of these
217 cells, many fragments (especially *apob-S*) still had fewer than five cells compared to control
218 fragments (Fig. 3c, d). These data suggested that *apob* inhibition delayed, but did not
219 completely abolish, re-establishment of these cells.

220 *apob* RNAi also affected regeneration of planarian organs, including the brain, pharynx,
221 and intestine. Although both brain and pharynx regenerated, these organs were smaller than in
222 controls (Supplementary Fig. 2g, h). This suggesting regeneration was delayed, but not blocked,
223 similar to the phenotype for cells expressing polarity cues. Quantitatively, at 6 dpa, both brain
224 and pharynx were smaller in size, especially in *apob-S* fragments (Fig. 3e, f). To assess
225 intestine, we analyzed both head and tail regenerates, in which a combination of neoblast-
226 driven new cell production and remodeling of pre-existing, differentiated intestinal branches is
227 required for successful regeneration[56]. Newly regenerated posterior branches were significantly
228 shorter in *apob(RNAi)* head fragments (Fig. 3g). By contrast, in tail fragments, length of the new
229 anterior intestine was not significantly affected (Fig. 3h). Rather, these branches failed to fuse at
230 the anterior midline, leading to a "split" anterior branch phenotype in ~50% of *apob(RNAi)* tail
231 fragments (Fig. 3h). Together, these results suggested that ApoB reduction delayed
232 regeneration of multiple cell types and organs, and, in the case of the intestine, affected
233 differentiation of new cells as well as collective cell migration or other processes required for
234 remodeling.

235

236 **_apob_ knockdown causes accumulation of early neoblast progeny**

237 Because *apob* knockdown disrupted multiple neoblast-driven processes during
238 regeneration, we asked whether defects in neoblast maintenance or proliferation were
239 responsible for the effects of *apob* RNAi on regeneration. First, we assessed neoblast numbers

240 by FISH using *piwi-1,* a pan-neoblast marker, and *tgs-1,* a marker for a more pluripotent
241 subpopulation (which also includes neural specialized neoblasts)[49,50,57]. In both uninjured
242 planarians and 7.5-day regenerates, neoblast numbers and distribution were grossly normal
243 (Supplementary Fig. 4a, b). We also assessed proliferation using anti-phospho-Histone H3
244 (Ser10) ("PS10") immunolabeling, which marks cells in late G2 and M phase of the cell
245 cycle[58,59]. In uninjured animals and 2-day head regenerates, the number of mitotic neoblasts
246 increased modestly in *apob-M,* but not *apob-S* samples (Fig. 4a, b). In 2-day trunk regenerates,
247 there was a more significant (~50%) increase in *apob-M* fragments, and a modest increase in
248 *apob-S* fragments (Fig. 4b). Together, these results suggested that ApoB reduction might cause
249 moderate hyperproliferation, or, alternatively, a modest mitotic delay, without dramatically
250 affecting *piwi-1+* or *tgs-1+* neoblast numbers. These mild phenotypes also raised the possibility
251 that ApoB reduction might preferentially dysregulate differentiation, rather than proliferation or
252 maintenance of actively cycling neoblasts.

253 We tested these possibilities quantitatively using flow cytometry. We dissociated
254 uninjured and regenerating planarians, and evaluated the proportions of cells in the X1 and X2
255 fractions (Fig. 4c). In uninjured planarians, as well as 2-day and 7-day regeneration fragments,
256 X1 neoblast numbers were unaffected by *apob* knockdown (Fig. 4d, e and Supplementary Fig.
257 4c), consistent with the moderate effect of *apob* RNAi on neoblast proliferation (Fig. 4a, b and
258 Supplementary Fig. 4a, b). By contrast, in uninjured planarians as well as 2- and 7-day trunk
259 fragments, the proportion of cells in the X2 gate increased significantly by ~20-40% (Fig. 4f and
260 Supplementary Fig. 4c) in *apob(RNAi)* animals vs. control. In 2 dpa head fragments, there was
261 also a modest, but statistically insignificant, increase (~15%) in the X2 fraction (Fig. 4f).
262 Because the X2 fraction includes both cycling G1-phase neoblasts and differentiating post-
263 mitotic progeny[60,61], these results suggested that *apob* inhibition might cause lengthening of G1
264 phase of the cell cycle, and/or a delay in differentiation of neoblast progeny, either of which
265 could increase the proportion of cells in X2.

266 In order to distinguish between these possibilities, we examined the X2 fraction in
267 uninjured planarians 24 hr after X-irradiation, which preferentially ablates over 95% radiation-
268 sensitive cycling neoblasts, without affecting many early neoblast progeny[49,52,60]. As expected,
269 the X1 fraction was almost completely eliminated in both control and *apob(RNAi)* samples (Fig.
270 4g, h). However, although irradiation reduced the proportion of X2 cells by ~48-56% in both
271 control and *apob(RNAi)* animals (Fig. 4i), the expansion of the X2 fraction persisted in *apob-M*
272 (~62.5% increase) and *apob-S* animals (~42.5% increase) relative to controls (Fig. 4i). This
273 increase in radiation-insensitive cells in X2 strongly suggested that the primary defect in *apob*
274 knockdown animals was a delay in differentiation of neoblast progeny.
275 Intriguingly, the increase in radiation-resistant X2 cells was transient: by 48 hr post-
276 irradiation, the proportion of X2 cells in *apob(RNAi)* samples was only modestly (but not
277 significantly) elevated (Fig. 4i). This suggested that differentiation was delayed, but not arrested,
278 in *apob(RNAi)* animals. One possible explanation for this observation is that, at later time points,
279 progeny had differentiated further, and resided in the Xins gate (rather than the X2 gate) as they
280 achieved a more mature cell state. Alternatively, some early progeny might have undergone
281 apoptosis or necrosis at later time points, reducing the apparent accumulation of neoblast
282 progeny in X2.
283
284 **ApoB reduction preferentially dysregulates expression of transcripts enriched in**
285 **differentiating neoblast progeny and mature cell types**
286 Our flow cytometry data suggested that the primary phenotype in uninjured and
287 regenerating *apob(RNAi*) animals was a delay in the differentiation of neoblast progeny. To test
288 this interpretation further, we performed whole animal RNA sequencing on control, *apob-M,* and
289 *apob-S* animals, and identified differentially expressed (DE) genes in the two *apob(RNAi)*
290 groups (Supplementary Fig. 5a-c and Supplementary Data 4). Then, to identify specific
291 biological processes affected by *apob* inhibition, we used the Gene Ontology (GO) to identify

292 patterns of dysregulation in specific functional categories (Supplementary Fig. 5d, e and
293 Supplementary Data 5). In addition, to determine whether *apob* knockdown disproportionately
294 dysregulated genes enriched in differentiating progeny states, we mapped the global *apob*
295 "dysregulation signature" to published bulk- and single-cell transcriptomes to determine which
296 cell types and states were most affected by *apob* inhibition.

297 *apob* knockdown dysregulated thousands of genes, causing upregulation of 842 (*apob*-
298 M) and 1960 (*apob-S)* transcripts, and downregulation of 1139 (*apob*-M) and 2547 *(apob*-S)
299 transcripts, relative to control (Supplementary Fig. 5a-c and Supplementary Data 4a-d). For
300 upregulated transcripts, "lipid metabolism" was the fifth-most over-represented Biological
301 Process (BP) term in *apob-M* animals, and was the most over-represented category in *apob-S*
302 animals (Supplementary Fig. 5d and Supplementary Data 5a, b). Enrichment of the
303 subcategories of acylglycerol, fatty acid, steroid, and glycerolipid metabolism was consistent
304 with known roles of ApoB orthologs, and suggested a possible compensatory gene expression
305 response to *apob(RNAi)*-induced disruption of NL transport. *apob(RNAi)* also downregulated
306 transcripts in additional metabolism categories, including gluconeogenesis, glycolysis, pyruvate,
307 and nucleotide metabolism (e.g., NADH and ADP), as well as ion transport, indicating wide-
308 ranging dysregulation of metabolite processing and trafficking, especially in *apob-S* animals
309 (Supplementary Fig. 5e and Supplementary Data 5c, d). Interestingly, *apob* inhibition
310 dysregulated many additional, non-metabolism-related transcripts. Upregulated functional
311 categories included differentiation and/or specification of multiple tissues including epidermis,
312 nervous system, and the eye, while downregulated categories included cilium morphogenesis
313 and function (possibly reflecting disruption of ciliated epidermal and/or protonephridial cell
314 numbers or physiology), muscle morphogenesis and function, and extracellular matrix
315 organization (Supplementary Fig. 5d, e and Supplementary Data 5a-d). Importantly, categories
316 related to cell cycle, mitosis, etc. were not enriched among up- or downregulated transcripts.
317 Together, these data suggested that ApoB reduction affected metabolism, cell/tissue

318 differentiation, and functions of mature cell types, but not processes required specifically for
319 cellular proliferation.

320 Next, to test whether *apob* disproportionately dysregulated genes expressed by
321 differentiating progeny and mature cells, we cross-referenced our DE transcript list with recently
322 published bulk transcriptomes from flow-sorted X1, X2, and Xins cell fractions (Fig. 4c)[49], as well
323 as cells sorted based on their expression of PIWI-1 protein, a widely used marker whose
324 expression marks states within planarian cell lineages (e.g., high PIWI-1 levels in neoblasts, low
325 PIWI-1 levels in some neoblasts and differentiating progeny, and negligible PIWI-1 levels in
326 mature cells)[49]. We first identified transcripts that were enriched in each cell fraction to generate
327 a "signature" transcript list for each fraction (Supplementary Fig. 6a, c). We then asked what
328 percent of these signature transcripts were dysregulated in *apob-M* and *apob-S* animals (Fig.
329 5a, b and Supplementary Fig. 6b, d). *apob* RNAi dysregulated signature transcripts in all six
330 fractions. However, compared to X1 or "PIWI-HI" signature transcripts, 2-4 times as many
331 transcripts were up- or down-regulated in X2 and "PIWI-LO" cell classes, which included both
332 neoblasts and early progeny (Fig. 5a, b). Relative to Xins and PIWI-NEG fractions, there were
333 also more dysregulated transcripts represented in the X2 and PIWI-LO fractions in *apob* RNAi
334 animals (Fig. 5a, b). To demonstrate the validity of this approach, we cross-referenced
335 transcriptomes from planarians 24 hours after irradiation[49], and found that dysregulated
336 transcripts overlapped mainly with X1 and PIWI-HI signature transcripts, and were primarily
337 downregulated, consistent with neoblast loss (Supplementary Fig. 6e, f). Together, this analysis
338 demonstrated that *apob* knockdown preferentially affected transcripts enriched in differentiating
339 progeny, an observation that is consistent with accumulation of cells in this state in flow
340 cytometry experiments (Fig. 4d-i).

341 To determine whether *apob* RNAi preferentially affected specific lineages or states within
342 individual lineages, we also compared the gene expression signature of *apob(RNAi)* animals
343 with recently published single cell transcriptomes[40]. Specifically, we cross-referenced transcripts

344 dysregulated by *apob* RNAi with transcripts enriched in cell state subclusters in eight planarian
345 lineages (Fig. 5c-i, Supplementary Fig. 8a, and Supplementary Fig. 8c-l). The resulting
346 "dysregulation signature" for each lineage showed how *apob* RNAi affected gene expression in
347 specific cell states during the progression from pluripotent cycling neoblasts ("N"), to early
348 transition states ("TS"), to differentiating progeny ("P") to mature cell states ("M") (see example
349 schematic for epidermal lineage in Fig. 5c). We observed a striking and consistent dysregulation
350 pattern in all eight lineages. In three well characterized lineages (epidermis, intestine, and
351 protonephridia) (Fig. 5c-i), the percentage of dysregulated "state-enriched" transcripts was
352 lowest for neoblast and early transition state subclusters, but higher for progeny and mature cell
353 states. Similar trends were observed for less characterized lineages such as muscle, pharynx,
354 and *cathepsin*-positive cells (Supplementary Fig. 8c-l). Validating this approach, irradiation[49]
355 primarily dysregulated neoblast and transition state transcripts (Supplementary Fig. 7a-g), and,
356 to a lesser degree for some lineages, progeny-enriched transcripts (Supplementary Fig. 8a and
357 Supplementary Fig. 8m-q). Similarly, and as expected, X1- and PIWI-HI-enriched transcripts
358 overlapped with neoblast and transition state transcripts, while X2-/PIWI-LO and Xins/PIWI-
359 NEG transcripts were enriched in progressively later cell state subclusters in each lineage
360 (Supplementary Fig. 7h-k, Supplementary Fig. 8b, and Supplementary Fig. 8r-v). Together,
361 these results provided further evidence that *apob* inhibition specifically dysregulated gene
362 expression in progeny and mature cell types/states in all eight lineages, and lent additional
363 support to the conclusion that ApoB was required for differentiation of planarian neoblasts.
364

365 ## Discussion

366 In this study, we discover a non-cell autonomous role for ApoB proteins in regulation of
367 planarian neoblast differentiation. Our data suggest that ApoB transports NLs from the intestine
368 to both neoblasts and their differentiating progeny via LPs (Fig. 6). In the absence of ApoB,
369 neoblast proliferation and maintenance are largely unaffected, but differentiation is delayed,
370 causing accumulation of differentiating progeny (Fig. 6) and slowing regeneration.

371 *apob* knockdown causes a ~40% increase in a flow cytometry fraction of 2C DNA
372 content cells (X2) that includes both cycling neoblasts in G1, and post-mitotic differentiating
373 progeny in G0[57,60]. This increase occurs without simultaneously affecting the >2C S/G2/M cell
374 fraction (X1), and is sustained even in recently irradiated animals, indicating that the expansion
375 is comprised primarily of G0 progeny, and not G1 neoblasts. We suggest that this phenotype
376 indicates a disruption in the progression of differentiation after cell fate specification, and not
377 specification itself. In planarians, specification likely begins during S-phase, because expression
378 of fate-specific transcription factors is significantly higher in S/G2/M neoblasts than in G1
379 neoblasts[57,62]. Intriguingly, inhibition of other planarian genes required for differentiation (e.g.,
380 the transcription factor *mex3-1,* the extracellular matrix component *collagen4-1,* and the
381 transcriptional co-activating protein *cbp-3*) also cause increases in neoblast numbers *in vivo*[52,63-
382 65]. Furthermore, knockdown of *exocyst component 3 (exoc3),* a negative regulator of
383 pluripotency whose mammalian homolog *Tnfaip3* promotes embryonic stem cell differentiation,
384 causes expansion of the S/G2/M (X1) neoblast fraction[66]. We speculate that these genes may
385 be required for cell fate specification, and that their inhibition shifts neoblast dynamics in favor of
386 renewal divisions that expand the stem cell compartment. By contrast,-*apob* RNAi does not
387 cause accumulation of S/G2/M neoblasts, but rather increases post-mitotic progeny number,
388 and causes greater dysregulation of transcripts associated with differentiation and mature cell
389 states. Therefore, ApoB is likely required to drive post-specification stages of differentiation, and

390 inhibition delays late commitment steps (i.e., after cell cycle exit), and/or transitions to final
391 mature states (Fig. 6).
392 Differentiation requires extensive changes in gene expression that are often preceded by
393 genome-wide chromatin remodeling[67,68]. Intriguingly, FA oxidation is a significant source of
394 carbon for acetyl-CoA production and histone acetylation[69]. Consistent with a role for NLs in
395 planarian differentiation, knockdown of *exoc3* reduces triglyceride levels, causes expansion of
396 the neoblast population, inhibits organogenesis, and reduces expression of differentiation
397 markers; palmitic acid supplementation rescues these differentiation-associated phenotypes[66].
398 Furthermore, in the sexually reproducing *S. mediterranea* planarian biotype, inhibition of *nuclear*
399 *hormone receptor 1* causes NL accumulation and blocks differentiation of gonads and
400 accessory reproductive tissues, a phenotype that is rescued by supplementation with either
401 acetyl-CoA or Acyl-CoA synthetase[70]. Because acetyl-CoA can also enter the citric acid cycle to
402 produce alpha-ketoglutarate, a substrate for histone demethylation[71], ApoB inhibition could
403 dysregulate epigenetic changes through multiple pathways. Histone acetylases, deacetylases,
404 methyltransferases, and demethylases are conserved in planarians, and their inhibition disrupts
405 stem cell maintenance, differentiation, and regeneration[64,65,72-75]. Because *apob* RNAi results in
406 widespread dysregulation of thousands of transcripts associated with differentiating progeny, it
407 is reasonable to suggest that in planarians, intestinal lipid stores serve as a ready carbon
408 source that is trafficked by ApoB-containing LPs to neoblasts and progeny to support epigenetic
409 modifications required for differentiation.
410 ApoB depletion may also delay differentiation by other mechanisms. For example, NL-
411 derived fatty acids may be utilized to produce ATP via beta-oxidation and the mitochondrial
412 electron transport chain (ETC) to support energy-dependent processes during differentiation.
413 Consistent with this idea, planarian mitochondrial mass is higher in differentiating progeny, and
414 pharmacological inhibition of the ETC promotes pluripotency and neoblast colony expansion,
415 which may also limit differentiation[76]. In mammals, disrupting the ETC blocks differentiation of

416 cardiomyocytes and mesenchymal stem cells[77,78], but the ETC is dispensable for differentiation
417 of mammalian epidermal progenitor cells and *Drosophila* ovarian stem cells[79,80]. Further study
418 will be needed to determine whether LP-transported NLs serve as a significant energy source
419 during planarian differentiation. Additionally, LP-mediated transport of morphogens like
420 Hedgehog or Wnt proteins[81], whose planarian orthologs play important roles in regulating axial
421 polarity and tissue differentiation[53], may be affected by *apob* knockdown. However, we find that
422 ApoB inhibition delays, but does not block or alter regeneration of axial polarity, and we find little
423 evidence of dysregulation of polarity-related transcripts (Supplementary Data 4 and 5),
424 suggesting that planarian LPs may not play a major role in planarian morphogen trafficking.
425 Similarly, fat-soluble vitamins known to influence stem cell dynamics are also transported in
426 LPs[82-87]. Although characterization of LP cargo may yield additional insights, the dramatic
427 dysregulation of lipid metabolism at the gene expression level, and the minimal disruption of
428 vitamin-related gene expression in *apob(RNAi)* animals (Supplementary Data 4 and 5), suggest
429 that LP-mediated vitamin transport may not play a significant role in planarian differentiation.
430 Lastly, we find that *apob* inhibition dysregulated genes associated with muscle differentiation
431 and function (Supplementary Data 5). In planarians, muscle cells not only secrete axial polarity
432 cues, but also serve a fibroblast-like role by secreting most components of the extracellular
433 matrix, whose functions are required to both spatially restrict the stem cell compartment, and
434 modulate proliferation and differentiation[63,88,89]. *apob* RNAi causes moderate downregulation of
435 most fibrillar collagens, as well as the basement membrane *collagen4-1,* which promotes
436 differentiation[63] (Supplementary Data 4 and 5). Thus, ApoB depletion may also delay
437 differentiation indirectly, by compromising the generation and/or function of muscle cells.
438 The effect of *apoB* knockdown on regeneration suggests several future directions. First,
439 although the existence of prominent LDs in planarian neoblasts has been known for decades[90],
440 the roles of this intriguing organelle have not been investigated. We did not assess neoblast LD
441 numbers or size, but *apoB* knockdown dramatically reduces NL content in both X1 (S/G2/M)

442 and X2 (G0/G1) neoblast fractions, suggesting that ApoB and LPs may influence neoblast LD
443 content and/or function. In addition, NL content is lower in G0/G1 cells, suggesting that a
444 primary role of LDs may be to support differentiation. Once thought of as static storage particles,
445 recent work has demonstrated that LDs in animal cells are dynamic, multi-functional organelles
446 that regulate nutrient sensing, cell stress responses, and even intracellular localization of
447 histones, transcription factors, and other proteins[2,10]. Additionally, although emerging data
448 suggest LDs as a potential therapeutic target in cancer stem cells [91,92], our knowledge of the
449 regulation and functions of LDs in stem cells, especially during regeneration, is limited. Studies
450 in planarians and other regeneration models could further illuminate the roles of this organelle.
451 Second, coordinated metabolic shifts between glycolysis and oxidative phosphorylation may be
452 a widespread aspect of stem cell transitions between quiescence, proliferation, and
453 differentiation, and extrinsic lipids can influence these states[11-14]. Our RNA-Seq data suggest
454 that transcription of regulators of amino acid metabolism, glycolysis, the tricarboxylic acid cycle,
455 and other metabolic pathways respond to *apob(RNAi)*, suggesting that planarian stem cell
456 metabolism is just as dynamic as in other animals. The fact that *apob(RNAi)* seems to primarily
457 affect post-mitotic states also suggests that planarian neoblasts might rely primarily on
458 glycolysis for energy and metabolite supply, and shift to lipid metabolism and oxidative
459 phosphorylation during differentiation, as in other systems[93-95]. Again, studies in animals with
460 high regenerative capacity could generate greater insights into whether and how injury can
461 induce metabolic switching. Third, we find that expression of *apob-1* and *apob-2,* as well as
462 numerous other regulators of NL metabolism are dynamically up- and down-regulated at the
463 transcript level during regeneration (Supplementary Fig. 3E). This suggests that coordination of
464 lipid metabolism is part of a genome-encoded program of regenerative gene expression.
465 Unraveling which transcription factors, chromatin modifiers, and other regulators are responsible
466 for such regulation is thus a third priority for future study.

467 Finally, because *apob-1* and *apob-2* are downregulated by inhibition of *nkx2.2,* an
468 intestine-enriched transcription factor also required for regeneration[39], our results provide a
469 specific example of how the planarian intestine can non-autonomously influence neoblast
470 dynamics. Intriguingly, unlike *nkx2.2* RNAi, *apob* knockdown does not reduce the abundance of
471 phosphoHistone-H3-S10-positive neoblasts, indicating that the proliferative defect in
472 *nkx2.2(RNAi)* animals is not caused by *apob* reduction, and additional downstream regulators of
473 proliferation remain to be discovered. Intriguingly, dozens of additional regulators of lipid
474 metabolism and transport of other metabolites are downregulated in *nkx2.2(RNAi)* animals
475 (Supplementary Data 1b), suggesting additional ways in which the intestine could influence
476 neoblasts and their niche.
477 In summary, we have identified *apolipoprotein B* orthologs and neutral lipid metabolism
478 as important regulators of stem cell differentiation and regenerative tissue growth. Since the
479 discovery of lipoproteins a century ago, their roles in lipid transport and disease have been
480 extensively investigated[96], but functions in stem cell regulation are not nearly as well
481 characterized[97-100]. Efforts to define functions of LPs and their metabolic derivatives more
482 precisely in planarians and other models will therefore improve our understanding of metabolic
483 requirements of stem cell-driven regeneration. In addition, because lipid metabolism is
484 amenable to pharmacological manipulation[101], further study may provide new insights relevant
485 to the dual goals of promoting repair of damaged human tissues, and inhibiting growth in
486 pathological contexts like cancer.
487

488 # Methods

489 **Ethics Statement**

490 Anti-ApoB-1 antibodies were generated by GenScript USA (Piscataway, NJ), an OLAW,
491 AAALAC, and PHS-approved vendor. GenScript's animal welfare protocols were approved by
492 OMRF IACUC (17-58). No other vertebrate organisms were used in this study.

493

494 **Planarian care**

495 Asexual *Schmidtea mediterranea* (clonal line CIW4)[102] were maintained in 0.5 g/L Instant
496 Ocean salts with 0.0167 g/L sodium bicarbonate dissolved in Type I water[103], and fed with beef
497 liver paste. Planarians were starved 7-10 days prior to initiating RNAi. Animals were 2-5 mm in
498 length for most experiments except flow cytometry, for which 5-10 mm animals were used.
499 Uninjured, intact animals were randomly selected from large (300-500 animal) pools.

500

501 **Cloning and expressed sequence tags**

502 Transcripts were cloned as previously described[104]. Sequences were identified in the
503 dd_Smed_v6 transcriptome[105] and the Smed_ESTs3 library[106]. These included *nkx2.2*
504 (dd_2716_0_1/PL08007A2A07),
505 *apob-1* (dd_636_0_1/PL06004B2E09), *apob-2* (dd_194_0_1/PL08004B1B10), *ldlr-1*
506 (dd_9829_0_1), *ldlr-2* (dd_5596_0_1/PL04021A1C10), *vldlr-1* (dd_1510_0_1/PL05007B1H03),
507 *notum* (dd_24180_0_1), *wnt11-2* (dd_16209_0_1), *choline acetyltransferase/ChAT*
508 (dd_6208_0_1), *laminin* (dd_8356_0_1/PL030015A20A02), *cathepsin La/ctsla*
509 (dd_2567_0_1/PL06020B2D09), *piwi-1* (dd_659_0_1/PL06008A2C06), *tgs-1* (dd_10988_0_1),
510 *solute carrier family 22 member 6/slc22a6* (dd_1159_0_1), and Niemann-Pick type C-2/*npc2*
511 (dd_73_0_1/PL030001B20C07). *S. mediterranea ldlr-1, ldlr-2,* and *vldlr-1* were identified by

512 BLAST homology and named after their top human refseq_protein BLASTX hits. Sequences of
513 primers and expressed sequence tags are available in Supplementary Data 6.
514
515 **Domain organization and phylogenetic analysis**
516 For ApoB-1, ApoB-2, Ldlr-1, Ldlr-2, and Vldrl-1, protein domains were identified using
517 HMMSCAN (https://www.ebi.ac.uk/Tools/hmmer/search/hmmscan) to search Pfam, TIGRFAM,
518 and Superfamily databases, with Phobius for transmembrane and signal peptide predictions
519 (conditional E-value cutoff of 1e-03)[107]. For the ApoB phylogenetic tree, N-terminal Vitellogenin
520 domains from ApoB and related proteins were aligned in Geneious using MAAFT (default
521 settings), and alignment was manually trimmed to the N- and C-terminal boundaries of human
522 Apo B-100. Phylogenetic tree was generated using PhyML 3.0[108] (http://www.atgc-
523 montpellier.fr/phyml/), using AIC for automatic selection of the LG substitution model, BioNJ
524 starting tree, NNI for tree topology improvement, and 100 bootstrap replicates. Accession
525 numbers for proteins used in domain diagrams and phylogenetic analysis are included in
526 Supplementary Data 6.
527
528 **In situ hybridization**
529 Riboprobe synthesis, WISH, and FISH were conducted as previously described[104].
530 Riboprobes were used at 0.05-1 ng/μl. Cryosections were generated after FISH as in[109].
531
532 **RNAi**
533 dsRNA synthesis and RNAi experiments were conducted as described[41,104] by mixing
534 one μg of in vitro-synthesized dsRNA with 8-9 μl of 1:10 food coloring:water mix, and 40 μl of
535 2:1 liver:water homogenate. For *nkx2.2* RNAi, animals were fed only once; RNA was extracted
536 for RNA-Seq after seven days. For *apob* RNAi, 2 μg control *egfp* dsRNA or 1 μg each *apob-1*

537 and *apob-2* (for simultaneous RNAi) were mixed with liver and food coloring, and animals were
538 fed 5 times for initial viability experiments, and 3-5 times for most other experiments, separating
539 animals with "mild" (*apob-M)* and "severe" *(apob-S)* phenotypes prior to fixation, amputation, or
540 flow cytometry. Non-eating planarians were always removed from the experiment if they refused
541 a second dsRNA feeding one day later.
542
543 **pH3-PS10 immunolabeling**
544 Mucus removal and fixation were conducted with 2% ice-cold HCl (3 min) and
545 methacarn at room temperature (RT, 20 min), followed by bleaching in 6% H_2O_2 in methanol as
546 in[109]. Fixed animals/regenerates were blocked (4 hr, RT) in IF block (1X PBS, 0.45% fish
547 gelatin, 0.6% IgG-free BSA, 0.3% Triton X-100), incubated in rabbit anti-phospho-Histone H3-
548 S10 at 1:2000 overnight (O/N, 4°C) (Cell Signaling 3377S), washed 8X in PBSTx (1X PBS plus
549 0.3% Triton X-100) (30 min each, RT), re-blocked for 1 hr, then incubated with goat anti-rabbit-
550 HRP (1:2000) (Jackson ImmunoResearch 111-035-003) (O/N, 4°C). Samples were again
551 washed 8X (20-30 min each, RT), then tyramide signal amplification (TSA) was conducted for
552 10 min as described[110] with TAMRA-tyramide. Samples were washed in PBSTx for two days,
553 then mounted in Vectashield (Vector Labs H-1000-10).
554
555 **Immunolabeling (cryosections)**
556 Cryosections (12 μm) of planarians relaxed in 0.66M $MgCl_2$ and fixed (O/N, 4°C) in 4%
557 formaldehyde (EM)/1X PBS were generated as described[109]. After rehydration, heat-mediated
558 antigen retrieval (10 min) in 10 mM sodium citrate, pH 6.0 was performed. Slides were
559 permeabilized for 30 min in 1X PBS/0.2% Tween-20, then blocked for 30 min at RT with 0.45%
560 fish gelatin and 0.6% BSA for 30 min in PBSTw (1X PBS, 0.05% Tween 20). Slides were
561 incubated with custom rabbit anti-ApoB-1 (1:1000, 0.59 μg/ml) and mouse 6G10 anti-muscle

562 (1:250 in block)[111] in blocking buffer (O/N, 4°C). Slides were washed three times (10 min, RT)
563 with PBSTw after antibody incubation. Slides were then incubated with goat anti-rabbit-HRP
564 (1:2000) (Jackson ImmunoResearch, 111-035-144) and goat anti-mouse-488 (1:250) (Jackson
565 ImmunoResearch, 115-545-146) at RT for 60 min. Slides were washed three times (in PBSTw),
566 with DAPI (2 μg/ml) counterstaining during the first wash. TSA was conducted for 10 min with
567 TAMRA-tyramide as described[110], followed by washes. Slides were mounted in Fluoromount G
568 (Southern Biotech).
569
570 **Anti-ApoB-1 antibody generation**
571 Sequence corresponding to the N-terminal Vitellogenin domain of ApoB-1 (dd_636,
572 nucleotides 45-1919, amino acids 1-625) was supplied to GenScript USA (Piscataway, NJ).
573 GenScript synthesized a plasmid encoding this region fused to KLH and a HIS tag, expressed
574 and purified the fusion protein, immunized New Zealand rabbits, affinity purified the antibody,
575 and assessed antibody titer and immunogenicity with both ELISA and Western blot.
576
577 **Protein extraction and Simple Western analysis**
578 5-10 planarians were rocked gently (40-50 rpm) for 7 min in 7.5% N-Acetyl-L-Cysteine
579 and rinsed 2X in 1X PBS. Samples were then homogenized using a motorized Kontes pestle
580 grinder in 250 μl RIPA (50 mM Tris pH 8.0, 150 mM NaCl, 1% NP-40, 0.5% sodium
581 deoxycholate, 0.5% SDS) with 40 mM DTT and 1X Halt Protease Inhibitor cocktail (Thermo
582 Scientific 78430). After 30 min on ice, samples were centrifuged (20,817 x *g,* 15 min, 4°C), and
583 supernatant was recovered and stored at -80°C. DTT concentration was reduced by buffer
584 exchange with RIPA (1 mM DTT) using Amicon Ultra 3 kDa columns (UFC500396), then protein
585 concentration was determined using a BCA kit (Pierce 23225) and DeNovix cuvet
586 spectrophotometer according to manufacturers' protocols. For Simple Western (ProteinSimple),

587 lysates were run according to the manufacturer's protocol on a Wes Instrument (running
588 Compass v4.0.0) at 0.1 mg/ml using the 66-440 kDa Wes Separation module (SM-W008) with
589 anti-ApoB-1 at 1:250 (~2.3 μg/ml). ApoB-1 peak areas were calculated with the following
590 settings: Range 10-600; Baseline Threshold 1.0, Window 15.0, and Stiffness 1.0; and Peak Find
591 Threshold 10.0 and Width 20.0 using the "Dropped Lines" method. Settings were identical for
592 total protein peak area, with these exceptions: Baseline Window 50.0 and Stiffness 0.5.
593 For the regeneration time course, ApoB-1 protein levels were run in biological triplicates,
594 normalized to total protein using the Wes Total Protein Detection Module (DM-TP01), and then
595 normalized to the "0 hour" time point in Excel.
596
597 **Oil Red O staining**
598 Planarians were relaxed in 0.66 M $MgCl_2$, fixed overnight (RT) in 4% formaldehyde (EM
599 grade) in 1X PBS, protected in sucrose, and cryosectioned (20 μm) onto SuperFrost Plus
600 slides[109]. Slides were rehydrated in deionized (DI) water (3 x 10 min, RT), then stained in Oil
601 Red O (Sigma O0625) solution (6 ml Whatman-filtered 0.5% Oil Red O in 100% isopropanol
602 plus 4 ml ultrapure water) for 15 min at RT. Slides were quickly dipped 3-5X in 60% isopropanol
603 to remove excess dye, then rinsed for 1 min in 60% isopropanol, then rinsed 1 min in DI water.
604 Slides were then rinsed in PBS-Tween-20 (0.01%, to prevent drying), then mounted in 90%
605 glycerol/1X PBS, and imaged within 2-3 days.
606
607 **Thin Layer Chromatography**
608 Ten planarians (5-8 mm) were placed in 1.7 ml microcentrifuge tubes with all planarian
609 salts removed, and the animals' mass was obtained. Lipids were then extracted using the Folch
610 method[112]. Briefly, 1 ml ice-cold 2:1 chloroform:methanol was added, then animals were
611 sonicated in ice water in a cup-horn sonicator (10 cycles of 5 second pulses at ~48-55W).

612 Samples were rocked at RT for 5 hr, then centrifuged (2 min at 16,000 x *g,* 4°C) to pellet
613 insoluble material. Supernatant was recovered to a new tube and stored at -80°C. 1 ml 2:1
614 chloroform:methanol was added to the pellet, re-sonicated, rocked overnight at RT, then
615 centrifuged as above. 0.2 volumes 0.9% NaCl (in water) was added to each extract, tubes were
616 inverted gently 10-15X to mix, vortexed for 10-15 sec, then centrifuged (2 min at 2,000 x *g,* RT).
617 Lower phases from each biological replicate (4 control and 4 *apob(RNAi)* replicates, 10 animals
618 each) were recovered, and speed-vacuumed (30°C x 60-90 min with spinning) to evaporate
619 solvent. Concentrated lipids were resuspended in 2 μl chloroform per mg animal mass (above)
620 and stored at -80°C (for less than 7 days). TLC was performed as previously described[113] with
621 slight modifications. 150Å silica gel HL 250 μl 20x20 cm plates (iChromatography 66011/Miles
622 Scientific P76011) were pre-equilibrated with 1:1 chloroform:methanol (~ 1 hr). After drying, 1 μl
623 lipids and 3 μl standards (30 μg mono-, di-, triglyceride mix, SUPELCO 1787-1AMP, plus 30 μg
624 cholesteryl palmitate, SIGMA C6072) were spotted onto the plates using TLC spotting
625 capillaries. Non-polar lipids were resolved with a 80:10:1 petroleum ether:ethyl ether:acetic acid
626 mix. After drying, TLC plates were sprayed with Primuline (SIGMA 206865) (1 mg/ml fresh stock
627 in ultrapure water, diluted 1:100 into 80 ml acetone plus 20 ml ultrapure water), dried, and
628 imaged on an Alpha Innotech chemiluminescent imager with Cy2 excitation/emission filters.
629 Peak areas in images were quantified in ImageJ/Fiji using the "Plot Lanes" function in the Gels
630 submenu (https://imagej.nih.gov/ij/docs/menus/analyze.html). Averages were calculated and
631 normalized to controls in Excel.
632
633 **RNA extraction, library preparation, and RNA sequencing**
634 Uninjured planarians and regenerating tissue fragments were homogenized in Trizol
635 using a motorized Kontes pestle grinder, and RNA was extracted using two chloroform
636 extractions and high-salt precipitation buffer according to the manufacturer's instructions. After

637 precipitation, solutions were transferred to Zymo RNA columns for DNAse treatment and
638 purification, according to manufacturer's instructions. RNA samples were analyzed using Agilent
639 RNA ScreenTape on an Agilent TapeStation 2200 according to manufacturer's protocol.
640 For analysis of gene expression in control vs. *nkx2.2(RNAi),* mRNA was enriched using
641 oligo-dT homopolymer beads, and libraries were generated using the Illumina Truseq Stranded
642 mRNA Library Prep Kit according to the manufacturer's protocol. Final libraries were assayed on
643 the Agilent TapeStation for appropriate size and quantity. Libraries were pooled in equimolar
644 amounts as ascertained by fluorometric analysis, then final pools were absolutely quantified
645 using qPCR on a Roche LightCycler 480 with Kapa Biosystems Illumina Library Quantification
646 Reagents. Paired-end (2x150 bp) sequence was generated on an Illumina NovaSeq 6000
647 instrument. 28M-43M reads were generated for each of three biological replicates per condition.
648 For analysis of gene expression in control, *apob-M,* and *apob-S* animals, total RNA for 4-6
649 biological replicates per condition was submitted to GENEWIZ (South Plainfield, NJ) for library
650 generation using NEB NEXT ULTRA library prep and RNA sequencing with standard Illumina
651 adapters. Paired-end (2x150 bp) sequence was generated on an Illumina HiSeq 4000
652 instrument; 19M - 26M reads were generated for each replicate.
653
654 **Read mapping**
655 For both *nkx2.2(RNAi)* and *apob(RNAi)* experiments, quality control and read mapping
656 to unique transcripts in dd_Smed_v6[104,105] were conducted with FastQC (v0.11.5)[114], BBDuk
657 (v35.66) (https://sourceforge.net/projects/bbmap/), and Bowtie2 (v2.3.1)[115]. BBDuk (v36.99)
658 settings for paired end reads: k=13 ktrim=r mink=11 qtrim=rl trimq=10 minlength=35 tbo tpe.
659 Bowtie2 (v2.3.1) for paired end reads was used for mapping, with "-a" multi-mapping and "--
660 local" soft-clipping allowed. For read summarization, the "featureCounts" utility in the Subread
661 package (v1.6.3)[116] was used with a custom ".SAF" file and options "-p -M -O -F SAF" to include
662 multi-mapping and multi-overlapping reads.

663 For mapping of X1/X2/Xins and PIWI-HI/-LO/-NEG bulk sequence, regeneration
664 fragment sequence, and whole animal 24 hr post-irradiation sequence[49], fastq files were
665 downloaded from NCBI GEO (GSE107874), mapped to dd_Smed_v6_unique using BBDuk and
666 Bowtie2, followed by count summarization using Samtools as previously described[104].
667
668 **Differential expression analysis**
669 Read counts matrices were imported into R, then analyzed in edgeR v3.8.6[117]. First, all
670 transcripts with counts per million (CPM) < 1 in three samples (*nxk2.2(RNAi),* Zeng X1/X2/Xins
671 data, and Zeng 24 hr irradiation data) or four samples (all others) (e.g., lowly expressed
672 transcripts) were excluded from further analysis. Next, after recalculation of library sizes,
673 samples were normalized using trimmed mean of M-values (TMM) method, followed by
674 calculation of common, trended, and tagwise dispersions. Finally, differentially expressed
675 transcripts were identified using the pairwise exact test (*nkx2.2(RNAi)* and *apob(RNAi)*
676 experiments, Zeng 24 hr irradiation data) or the generalized linear model (GLM) likelihood ratio
677 test (other Zeng datasets). Expression changes were considered to be significant if the false
678 discovery rate adjusted *p* value ("FDR") was <.05.
679
680 **Gene Ontology analysis**
681 GO analysis was conducted using BiNGO[118] using a custom *S. mediterranea* GO
682 annotation as previously described[104]. RefSeq protein collections used for BLASTX and
683 UniProtKB Biological Process GO terms used for annotation were downloaded for each
684 organism in April 2020.
685
686 **Hierarchical clustering and heat maps**

687 Hierarchical clustering of transcripts annotated with lipid-metabolism-related GO terms
688 was conducted using EdgeR-generated log_2FC values in Cluster 3.0[119], with Euclidean distance
689 and complete linkage. Heat maps were generated with Java Treeview[120].
690
691 **qRT-PCR**
692 Total RNA was extracted from biological triplicates (5-10 animals/fragments per
693 replicate) using Trizol as for RNA-Seq samples. RNA was reverse transcribed using the iScript
694 cDNA Synthesis kit (BioRad 1708890). *apob-1* and *apob-2* levels were detected using the Fast
695 Start Essential Green DNA master mix (Roche 06924204001) on a Roche LightCycler 96
696 instrument. RNA levels were normalized to the geometric mean of endogenous controls *ef-2*
697 and *gapdh* using the Livak ΔΔCt method[121].
698
699 **Flow cytometry**
700 Planarians were dissociated and filtered in CMFB with collagenase as described[62]. Cells
701 were labeled at RT with Hoechst 33342 (50 μg/ml) for 45 min, followed by addition of propidium
702 iodide (1 μg/ml). For neutral lipid labeling, BODIPY 493/503 (Molecular Probes D3922) at 10
703 ng/ml was included with Hoechst. Cells were analyzed on a Becton Dickinson FACSCelesta
704 instrument with 405 nm, 488 nm, and 640 nm lasers. After gating for live cell singlets
705 (Supplementary Fig. 9a-c), X1, X2, and Xins gates were drawn using two criteria: cell
706 proportions were approximately 15% (X1) 25% (X2) and 60% (Xins), and reductions in X1 and
707 X2 fractions in 4-day post-irradiation animals were >95% and ~70%, respectively. Data were
708 analyzed and plots were generated in FloJo (v10.7.1). For irradiation, uninjured planarians were
709 dosed with 60 Grays (6,000 rads) using RS-2000 Biological Research X-Ray Irradiator (Rad
710 Source, Buford, GA).
711

712 **Cross-referencing of *apob(RNAi)* RNA-Seq data with published transcriptomes**

713 For comparison of dysregulated transcripts in *apob-M* and *apob-S* animals with bulk
714 neoblast transcriptome data[49], we first identified "signature" transcripts as follows. “X1
715 signature” transcripts were defined as those with a $\log_2$FC>0 (FDR<.05) compared to both “X2”
716 and “Xins.” “X2 signature” transcripts had $\log_2$FC>0 (fdr<.05) vs. both “X1” and “Xins.” “Xins
717 signature” had $\log_2$FC>0 (fdr<.05) vs. both “X1” and “X2.” Similarly, "PIWI-HI signature"
718 transcripts were defined as those with a $\log_2$FC>0 (fdr<.05) compared to both "PIWI-LO" and
719 "PIWI-NEG." "PIWI-LO signature" transcripts had $\log_2$FC>0 (fdr<.05) vs. both “PIWI-HI” and
720 “PIWI-NEG.” "PIWI-NEG signature" transcripts had $\log_2$FC>0 (fdr<.05) vs. both “PIWI-HI” and
721 “PIWI-LO.” Next, we used the "merge" function and "VennDiagram" package in RStudio
722 (v1.2.1335) to identify signature transcripts in X1/X2/Xins or PIWI-HI/-LO/-NEG that were also
723 dsyregulated (up or down) in *apob-M* or *apob-S* animals, as shown in Fig. S6. "% of
724 dysregulated transcripts" was calculated as the number of overlapping transcripts divided by the
725 total number of X1/X2/Xins or PIWI-HI/-LO/-NEG transcripts.

726 For comparison of dysregulated transcripts in *apob-M* and *apob-S* animals with single
727 cell type/state data in[40], we again used the "merge" function in RStudio to identify the number of
728 transcripts enriched in individual lineage subclusters (Table S2)[40] that were also dysregulated
729 by *apob* RNAi. "% of dysregulated transcripts" was calculated as the number of overlapping
730 transcripts divided by the total number of transcripts in each individual subcluster. In Fig. 5, the
731 "N/TS" (Neoblast/Transition State) designation included subclusters with high *piwi-1* mRNA
732 expression thought to be neoblast/progenitor subpopulations in epidermal, intestine, and
733 protonephridia lineages based on the conclusions of Fincher et al. and other published
734 data[45,62,122-124]. Similarly, the "P" (Progeny) and "M" (Mature) designations were based on
735 conclusions from both single cell RNA-Seq data and previous work. For lineages that are less
736 well understood *in vivo* (Fig. S8), we designated subclusters/states using both transcript
737 dysregulation in 24 hr irradiated animals [49] and *piwi-1* mRNA levels in t-SNE plots[40]. "N/TS"

738 subclusters possessed the greatest number of irradiation-dysregulated transcripts and the
739 highest *piwi-1* expression; "P" subclusters possessed fewer (by proportion) irradation-
740 dysregulated transcripts and lower *piwi-1* expression; and "M" subclusters had the fewest
741 radiation-sensitive transcripts and negligible *piwi-1* expression.
742
743 **Image Collection and Quantification**
744 Epifluorescent images (FISH samples) were collected on a Zeiss AxioObserver.Z1 with
745 Excelitas X-Cite 120 LED Boost illumination and Zen 2.3 pro. For quantification of pharynx and
746 brain size, organ area and animal area were measured in ImageJ[125] and organ-to-body size
747 ratios were calculated. For intestine, length of anterior branch and posterior branches were
748 measured in ImageJ. Means of posterior branch length were calculated, and then posterior-to-
749 anterior (head fragments) or anterior-to-posterior (tail fragments) length ratio was calculated.
750 For tail fragments with split anterior branch, anterior branch length was measured from the
751 anterior of the pharynx to the tip of the anterior-most primary branch. For tail fragments, the split
752 anterior branch phenotype (failure to fuse at the midline) was scored if there was an obvious
753 gap between anterior branches for at least half the length of the anterior branch. For images of
754 *apob-1* and *apob-2* FISH on cryosections, z-stacks were collected with an Apotome.2 for
755 generation of maximum orthogonal projections.
756 For anti-pH3-PS10-labeled samples, z-stacks were collected on a Zeiss
757 AxioObserver.Z1 at 10X magnification, followed by tile stitching, extended depth of focus
758 projection, and background subtraction (PS10 channel only) with a radius of 30. Control and
759 experimental samples to be compared were imaged at identical exposures. For quantification,
760 animal area and PS10+ nuclei were quantified using the Automated Segmentation tools in Zen
761 2.3 pro. Briefly, animal area was measured with Gaussian smoothing, no background
762 subtraction or sharpening, Morphology separation, and custom threshold settings that were the
763 same for all samples to be directly compared. PS10+ nuclei number was measured using

764 Lowpass smoothing, Rolling Ball background subtraction, Delineate sharpening, Watersheds
765 separation, with threshold settings and other parameters that were identical for all samples to be
766 directly compared. Number of mitoses per area were calculated for each animal/fragment.
767 Confocal images were collected on a Zeiss LSM 710 or LSM 880 laser scanning
768 microscope with 10X Plan NeoFluar, 20X Plan Apo, or 40X C-Apo objectives. For orthogonal
769 projections (anti-ApoB1 immunolabeling and *ldlr/vldlr* FISH), between three and ten z-planes
770 were collected at 1-2X "optimal" section thickness (based on objective NA). For *notum* and
771 *wnt11-2* FISH, full fragment thickness stacks were projected to ensure that all mRNA-positive
772 cells were counted.
773 Images of Oil-Red-O-stained sections, live animals, live regenerates, and WISH samples
774 were collected on a Zeiss Stemi 508 with an Axiocam 105 color camera, or a Zeiss Axio
775 Zoom.V16 with an Axiocam 105 camera. In some cases brightness and/or contrast were
776 adjusted in Adobe Photoshop to improve signal contrast.
777
778 **Statistics**
779 Detailed data and information regarding statistical testing are included in Source Data 2.
780 For experiments with statistical analysis, n values are indicated exactly by the number of data
781 points in figure plots, along with definitions of error bars and *p* or *q* values; all tests were
782 conducted in Prism 9 (GraphPad Software, San Diego, CA). For one-way ANOVA, ordinary
783 ANOVA was performed unless Brown-Forsythe and Bartlett's tests indicated standard
784 deviations were significantly different, then Brown-Forsythe and Welch ANOVA tests were
785 performed. For two-way ANOVA (flow cytometry experiments with irradiation), *q* values (FDR-
786 adjusted *p* values) were reported when interaction between RNAi condition ("Genotype") and
787 irradiation was significant (X2 subpopulation). Otherwise, *p* values were derived using one-way
788 ANOVA. *p* values of <.05 (*), <.01 (**), <.001 (***), and <0.0001 (****) were annotated with
789 asterisks in figures.

790 Replicate information for other experiments: polarity marker analysis, 5-15 fragments per
791 condition; for WISH and FISH, images are representative of 3-6 individual animals or fragments;
792 for anti-ApoB1 and Oil Red O labeling, images are representative of sections from 2-3
793 fragments/animals, and of at least two repeated experiments.
794 For statistical testing of overlap between genes dysregulated in *apob(RNAi)* planarians
795 and other RNA-Seq data sets, the R Package GeneOverlap[126] was used to conduct Fisher's
796 exact test on each comparison. Total number of detected transcripts ("genome size" in
797 GeneOverlap) was determined conservatively by only including transcripts detected in both
798 *apob* RNA-Seq and bulk[49] or single cell[40] sequencing data. For sc-RNA-Seq, the digital
799 expression matrix in GEO GSE111764 was normalized in Seurat as in Fincher et al.[40]; only
800 transcripts with non-zero expression in 0.5% of cells (Fincher TableS1) in each subcluster were
801 considered to be detected. p values <0.05 are indicated with a caret (^) in figures.
802 Replicate and statistical information for RNA-Seq and other bioinformatics experiments
803 are detailed in appropriate Methods sections.
804
805 **Data availability**
806 Raw and processed RNA-Seq data associated with this study will be made available in
807 the NCBI Gene Expression Omnibus (GEO) upon publication. Other data supporting this study's
808 findings are available within the article and its Supplementary files, or are available from the
809 authors upon reasonable request.
810
811 **Reporting summary**
812 Further information on research design is available in the Nature Research Reporting
813 Summary linked to this article.
814
815 **Competing interests**

816 The authors declare no competing financial interests.

817

818 ## Acknowledgments

819 We are very grateful to Phil Newmark (HHMI and the Morgridge Institute for Research),
820 in whose laboratory this project was initiated. We thank members of the Newmark and
821 Forsthoefel labs, and OMRF colleagues Pat Gaffney, Linda Thompson, Dean Dawson, and Hui-
822 Ying Lim for insightful discussions. We thank Jochen Rink, James Cleland, and Hanh Vu (Max
823 Planck Institute for Biophysical Chemistry) for sharing planarian protein extraction protocols,
824 Vasileios Morkotinis for *tgs-1* plasmid, and Rachel Roberts-Galbraith (Univ. of Georgia) for
825 *notum* and *wnt11-2* plasmids. We thank Steve Farber (Carnegie Institution for Science) for
826 advice on lipid extraction and TLC, and Jayhun Lee (Morgridge) for collaborative development
827 of planarian lipid analysis protocols. We are grateful to Hadi Maktabi (ProteinSimple) and to
828 OMRF colleagues Summer Wang and Lin Wang for help in developing Wes protocols; and to
829 members of the OMRF Flow Cytometry Core (Jacob Bass and Diana Hamilton), the
830 Quantitative Analysis Core (Lori Garman and Nathan Pezant), the Imaging and Histology Core,
831 the Clinical Genomics Core, the Gnotobiotic Mouse Core (for use of X-irradiator), and
832 IT/Research Computing Services for invaluable technical assistance. JRO was supported by the
833 Summer Research Opportunities Program at the University of Illinois at Urbana-Champaign.
834 This work was supported by NIH Centers of Biomedical Research Excellence (COBRE)
835 GM103636 (Project 1 to DJF), and the Oklahoma Medical Research Foundation.
836

837 ## Author Contributions

838 Conception and design of the project: DJF and LLW; data collection: CGB, LLW, JRO, NIC, and
839 DJF; data analysis and visualization: CGB, LLW, NIC and DJF; data interpretation: LLW, CGB,
840 and DJF; RNA-seq analysis: DJF; manuscript preparation: DJF, LLW, and CGB.
841

References

1 Walther, T. C., Chung, J. & Farese, R. V., Jr. Lipid Droplet Biogenesis. *Annu. Rev. Cell. Dev. Biol.* **33**, 491-510, doi:10.1146/annurev-cellbio-100616-060608 (2017).

2 Olzmann, J. A. & Carvalho, P. Dynamics and functions of lipid droplets. *Nat. Rev. Mol. Cell Biol.* **20**, 137-155, doi:10.1038/s41580-018-0085-z (2019).

3 D'Andrea, S. Lipid droplet mobilization: The different ways to loosen the purse strings. *Biochimie* **120**, 17-27, doi:10.1016/j.biochi.2015.07.010 (2016).

4 Guo, Y., Cordes, K. R., Farese, R. V., Jr. & Walther, T. C. Lipid droplets at a glance. *J. Cell Sci.* **122**, 749-752, doi:10.1242/jcs.037630 (2009).

5 Olofsson, S. O., Asp, L. & Borén, J. The assembly and secretion of apolipoprotein B-containing lipoproteins. *Curr Opin Lipidol* **10**, 341-346, doi:10.1097/00041433-199908000-00008 (1999).

6 Heier, C. & Kühnlein, R. P. Triacylglycerol Metabolism in Drosophila melanogaster. *Genetics* **210**, 1163-1184, doi:10.1534/genetics.118.301583 (2018).

7 Wong, L. H., Gatta, A. T. & Levine, T. P. Lipid transfer proteins: the lipid commute via shuttles, bridges and tubes. *Nat. Rev. Mol. Cell Biol.* **20**, 85-101, doi:10.1038/s41580-018-0071-5 (2019).

8 Lafontan, M. & Langin, D. Lipolysis and lipid mobilization in human adipose tissue. *Prog Lipid Res* **48**, 275-297, doi:10.1016/j.plipres.2009.05.001 (2009).

9 Ruggles, K. V., Turkish, A. & Sturley, S. L. Making, baking, and breaking: the synthesis, storage, and hydrolysis of neutral lipids. *Annu. Rev. Nutr.* **33**, 413-451, doi:10.1146/annurev-nutr-071812-161254 (2013).

10 Welte, M. A. & Gould, A. P. Lipid droplet functions beyond energy storage. *Biochim Biophys Acta Mol Cell Biol Lipids* **1862**, 1260-1272, doi:10.1016/j.bbalip.2017.07.006 (2017).

11 Ly, C. H., Lynch, G. S. & Ryall, J. G. A Metabolic Roadmap for Somatic Stem Cell Fate. *Cell Metab* **31**, 1052-1067, doi:10.1016/j.cmet.2020.04.022 (2020).

12 Ito, K. & Suda, T. Metabolic requirements for the maintenance of self-renewing stem cells. *Nat. Rev. Mol. Cell Biol.* **15**, 243-256, doi:10.1038/nrm3772 (2014).

13 Shyh-Chang, N. & Ng, H. H. The metabolic programming of stem cells. *Genes Dev.* **31**, 336-346, doi:10.1101/gad.293167.116 (2017).

14 Clémot, M., Sênos Demarco, R. & Jones, D. L. Lipid Mediated Regulation of Adult Stem Cell Behavior. *Front Cell Dev Biol* **8**, 115, doi:10.3389/fcell.2020.00115 (2020).

15 Ito, K. *et al.* A PML-PPAR-delta pathway for fatty acid oxidation regulates hematopoietic stem cell maintenance. *Nat. Med.* **18**, 1350-1358, doi:10.1038/nm.2882 (2012).

878 16 Knobloch, M. *et al.* A Fatty Acid Oxidation-Dependent Metabolic Shift Regulates Adult
879 Neural Stem Cell Activity. *Cell Rep* **20**, 2144-2155, doi:10.1016/j.celrep.2017.08.029
880 (2017).

881 17 Singh, S. R. *et al.* The lipolysis pathway sustains normal and transformed stem cells in
882 adult Drosophila. *Nature* **538**, 109-113, doi:10.1038/nature19788 (2016).

883 18 Sênos Demarco, R., Uyemura, B. S., D'Alterio, C. & Jones, D. L. Mitochondrial fusion
884 regulates lipid homeostasis and stem cell maintenance in the Drosophila testis. *Nat. Cell*
885 *Biol.* **21**, 710-720, doi:10.1038/s41556-019-0332-3 (2019).

886 19 Tiwari, S. K., Toshniwal, A. G., Mandal, S. & Mandal, L. Fatty acid beta-oxidation is
887 required for the differentiation of larval hematopoietic progenitors in Drosophila. *Elife* **9**,
888 doi:10.7554/eLife.53247 (2020).

889 20 Knobloch, M. *et al.* Metabolic control of adult neural stem cell activity by Fasn-dependent
890 lipogenesis. *Nature* **493**, 226-230, doi:10.1038/nature11689 (2013).

891 21 Driver, A. M., Kratz, L. E., Kelley, R. I. & Stottmann, R. W. Altered cholesterol
892 biosynthesis causes precocious neurogenesis in the developing mouse forebrain.
893 *Neurobiol Dis* **91**, 69-82, doi:10.1016/j.nbd.2016.02.017 (2016).

894 22 Cornacchia, D. *et al.* Lipid Deprivation Induces a Stable, Naive-to-Primed Intermediate
895 State of Pluripotency in Human PSCs. *Cell Stem Cell* **25**, 120-136 e110,
896 doi:10.1016/j.stem.2019.05.001 (2019).

897 23 Kang, J. *et al.* Modulation of tissue repair by regeneration enhancer elements. *Nature*
898 **532**, 201-206, doi:10.1038/nature17644 (2016).

899 24 Monnot, M. J. *et al.* Epidermal expression of apolipoprotein E gene during fin and scale
900 development and fin regeneration in zebrafish. *Dev. Dyn.* **214**, 207-215,
901 doi:10.1002/(SICI)1097-0177(199903)214:3<207::AID-AJA4>3.0.CO;2-5 (1999).

902 25 Voss, S. R. *et al.* Gene expression during the first 28 days of axolotl limb regeneration I:
903 Experimental design and global analysis of gene expression. *Regeneration (Oxf)* **2**, 120-
904 136, doi:10.1002/reg2.37 (2015).

905 26 Hayashi, H., Campenot, R. B., Vance, D. E. & Vance, J. E. Glial lipoproteins stimulate
906 axon growth of central nervous system neurons in compartmented cultures. *J. Biol.*
907 *Chem.* **279**, 14009-14015, doi:10.1074/jbc.M313828200 (2004).

908 27 Pauta, M. *et al.* Impaired liver regeneration in Ldlr-/- mice is associated with an altered
909 hepatic profile of cytokines, growth factors, and lipids. *J Hepatol* **59**, 731-737,
910 doi:10.1016/j.jhep.2013.05.026 (2013).

911 28 Tamilarasan, K. P. *et al.* Skeletal muscle damage and impaired regeneration due to LPL-
912 mediated lipotoxicity. *Cell Death Dis* **3**, e354, doi:10.1038/cddis.2012.91 (2012).

913 29 Pala, F. *et al.* Distinct metabolic states govern skeletal muscle stem cell fates during
914 prenatal and postnatal myogenesis. *J. Cell Sci.* **131**, doi:10.1242/jcs.212977 (2018).

30 Shook, B. A. *et al.* Dermal Adipocyte Lipolysis and Myofibroblast Conversion Are Required for Efficient Skin Repair. *Cell Stem Cell* **26**, 880-895 e886, doi:10.1016/j.stem.2020.03.013 (2020).

31 Newmark, P. A. & Sánchez Alvarado, A. Not your father's planarian: a classic model enters the era of functional genomics. *Nat. Rev. Genet.* **3**, 210-219, doi:10.1038/nrg759 (2002).

32 Reddien, P. W. & Sánchez Alvarado, A. Fundamentals of planarian regeneration. *Annu. Rev. Cell Dev. Biol.* **20**, 725-757 (2004).

33 Willier, B. H., Hyman, L. H. & Rifenburgh, S. A. A histochemical study of intracellular digestion in triclad flatworms. *Journal of Morphology and Physiology* **40**, 299-340, doi:DOI 10.1002/jmor.1050400205 (1925).

34 Jennings, J. B. Studies on feeding, digestion, and food storage in free-living flatworms (Platyhelminthes: Turbellaria). *Biol. Bull.* **112**, 63-80 (1957).

35 Mak, H. Y. Lipid droplets as fat storage organelles in Caenorhabditis elegans: Thematic Review Series: Lipid Droplet Synthesis and Metabolism: from Yeast to Man. *J. Lipid Res.* **53**, 28-33, doi:10.1194/jlr.R021006 (2012).

36 Gamo, J. & Garcia-Corrales, P. Ultrastructural changes in the gastrodermal phagocytic cells of the freshwater planarian *Dugesia gonocephala* s.l. during starvation. *J. Submicrosc. Cytol.* **19**, 291-302 (1987).

37 Thommen, A. *et al.* Body size-dependent energy storage causes Kleiber's law scaling of the metabolic rate in planarians. *Elife* **8**, doi:10.7554/eLife.38187 (2019).

38 Palm, W. & Rodenfels, J. Understanding the role of lipids and lipoproteins in development. *Development* **147**, doi:10.1242/dev.186411 (2020).

39 Forsthoefel, D. J. *et al.* An RNAi screen reveals intestinal regulators of branching morphogenesis, differentiation, and stem cell proliferation in planarians. *Dev. Cell* **23**, 691-704, doi:10.1016/j.devcel.2012.09.008 (2012).

40 Fincher, C. T., Wurtzel, O., de Hoog, T., Kravarik, K. M. & Reddien, P. W. Cell type transcriptome atlas for the planarian *Schmidtea mediterranea*. *Science* **360**, doi:10.1126/science.aaq1736 (2018).

41 Rouhana, L. *et al.* RNA interference by feeding in vitro-synthesized double-stranded RNA to planarians: methodology and dynamics. *Dev. Dyn.* **242**, 718-730, doi:10.1002/dvdy.23950 (2013).

42 Reddien, P. W., Bermange, A. L., Murfitt, K. J., Jennings, J. R. & Sánchez Alvarado, A. Identification of genes needed for regeneration, stem cell function, and tissue homeostasis by systematic gene perturbation in planaria. *Dev. Cell* **8**, 635-649, doi:10.1016/j.devcel.2005.02.014 (2005).

951 43 Palm, W. *et al.* Lipoproteins in Drosophila melanogaster--assembly, function, and
952 influence on tissue lipid composition. *PLoS Genet.* **8**, e1002828,
953 doi:10.1371/journal.pgen.1002828 (2012).

954 44 Young, S. G. Recent progress in understanding apolipoprotein B. *Circulation* **82**, 1574-
955 1594, doi:10.1161/01.cir.82.5.1574 (1990).

956 45 Wagner, D. E., Wang, I. E. & Reddien, P. W. Clonogenic neoblasts are pluripotent adult
957 stem cells that underlie planarian regeneration. *Science* **332**, 811-816,
958 doi:10.1126/science.1203983 (2011).

959 46 Hayashi, T., Asami, M., Higuchi, S., Shibata, N. & Agata, K. Isolation of planarian X-ray-
960 sensitive stem cells by fluorescence-activated cell sorting. *Dev. Growth Differ.* **48**, 371-
961 380, doi:10.1111/j.1440-169X.2006.00876.x (2006).

962 47 Wenemoser, D. & Reddien, P. W. Planarian regeneration involves distinct stem cell
963 responses to wounds and tissue absence. *Dev. Biol.* **344**, 979-991,
964 doi:10.1016/j.ydbio.2010.06.017 (2010).

965 48 Wurtzel, O. *et al.* A generic and cell-type-specific wound response precedes
966 regeneration in planarians. *Dev. Cell* **35**, 632-645, doi:10.1016/j.devcel.2015.11.004
967 (2015).

968 49 Zeng, A. *et al.* Prospectively Isolated Tetraspanin(+) Neoblasts Are Adult Pluripotent
969 Stem Cells Underlying Planaria Regeneration. *Cell* **173**, 1593-1608 e1520,
970 doi:10.1016/j.cell.2018.05.006 (2018).

971 50 Reddien, P. W., Oviedo, N. J., Jennings, J. R., Jenkin, J. C. & Sánchez Alvarado, A.
972 SMEDWI-2 is a PIWI-like protein that regulates planarian stem cells. *Science* **310**, 1327-
973 1330, doi:10.1126/science.1116110 (2005).

974 51 Scimone, M. L., Meisel, J. & Reddien, P. W. The Mi-2-like *Smed-CHD4* gene is required
975 for stem cell differentiation in the planarian *Schmidtea mediterranea*. *Development* **137**,
976 1231-1241, doi:dev.042051 [pii]
977 10.1242/dev.042051 (2010).

978 52 Zhu, S. J., Hallows, S. E., Currie, K. W., Xu, C. & Pearson, B. J. A *mex3* homolog is
979 required for differentiation during planarian stem cell lineage development. *Elife* **4**,
980 e07025, doi:10.7554/eLife.07025 (2015).

981 53 Reddien, P. W. The Cellular and Molecular Basis for Planarian Regeneration. *Cell* **175**,
982 327-345, doi:10.1016/j.cell.2018.09.021 (2018).

983 54 Petersen, C. P. & Reddien, P. W. Polarized notum activation at wounds inhibits Wnt
984 function to promote planarian head regeneration. *Science* **332**, 852-855,
985 doi:10.1126/science.1202143 (2011).

986 55 Adell, T., Saló, E., Boutros, M. & Bartscherer, K. Smed-Evi/Wntless is required for β-
987 catenin-dependent and -independent processes during planarian regeneration.
988 *Development* **136**, 905-910, doi:10.1242/dev.033761 (2009).

989 56 Forsthoefel, D. J., Park, A. E. & Newmark, P. A. Stem cell-based growth, regeneration,
990 and remodeling of the planarian intestine. *Dev. Biol.* **356**, 445-459,
991 doi:10.1016/j.ydbio.2011.05.669 (2011).

992 57 Raz, A. A., Wurtzel, O. & Reddien, P. W. Planarian stem cells specify fate yet retain
993 potency during the cell cycle. *Cell Stem Cell*, doi:10.1016/j.stem.2021.03.021 (2021).

994 58 Hendzel, M. J. *et al.* Mitosis-specific phosphorylation of histone H3 initiates primarily
995 within pericentromeric heterochromatin during G2 and spreads in an ordered fashion
996 coincident with mitotic chromosome condensation. *Chromosoma* **106**, 348-360 (1997).

997 59 Newmark, P. A. & Sánchez Alvarado, A. Bromodeoxyuridine specifically labels the
998 regenerative stem cells of planarians. *Dev. Biol.* **220**, 142-153,
999 doi:10.1006/dbio.2000.9645 (2000).

1000 60 Eisenhoffer, G. T., Kang, H. & Sánchez Alvarado, A. Molecular analysis of stem cells
1001 and their descendants during cell turnover and regeneration in the planarian *Schmidtea*
1002 *mediterranea*. *Cell Stem Cell* **3**, 327-339, doi:S1934-5909(08)00336-6 [pii]
1003 10.1016/j.stem.2008.07.002 (2008).

1004 61 Hayashi, T. *et al.* Single-cell gene profiling of planarian stem cells using fluorescent
1005 activated cell sorting and its "index sorting" function for stem cell research. *Dev. Growth*
1006 *Differ.* **52**, 131-144, doi:DGD1157 [pii]
1007 10.1111/j.1440-169X.2009.01157.x (2010).

1008 62 van Wolfswinkel, J. C., Wagner, D. E. & Reddien, P. W. Single-cell analysis reveals
1009 functionally distinct classes within the planarian stem cell compartment. *Cell Stem Cell*
1010 **15**, 326-339, doi:10.1016/j.stem.2014.06.007 (2014).

1011 63 Chan, A., Ma, S., Pearson, B. J. & Chan, D. Collagen IV differentially regulates planarian
1012 stem cell potency and lineage progression. *Proc Natl Acad Sci U S A* **118**,
1013 doi:10.1073/pnas.2021251118 (2021).

1014 64 Stelman, C. R., Smith, B. M., Chandra, B. & Roberts-Galbraith, R. H. CBP/p300
1015 homologs CBP2 and CBP3 play distinct roles in planarian stem cell function. *Dev. Biol.*
1016 **473**, 130-143, doi:10.1016/j.ydbio.2021.02.004 (2021).

1017 65 Fraguas, S. *et al.* CREB-binding protein (CBP) gene family regulates planarian survival
1018 and stem cell differentiation. *Dev. Biol.* **476**, 53-67, doi:10.1016/j.ydbio.2021.02.008
1019 (2021).

1020 66 Deb, S. *et al.* Tnfaip2/exoc3-driven lipid metabolism is essential for stem cell
1021 differentiation and organ homeostasis. *EMBO Rep*, e49328,
1022 doi:10.15252/embr.201949328 (2020).

1023 67 Yadav, T., Quivy, J. P. & Almouzni, G. Chromatin plasticity: A versatile landscape that
1024 underlies cell fate and identity. *Science* **361**, 1332-1336, doi:10.1126/science.aat8950
1025 (2018).

1026 68 Duncan, E. M. & Sánchez Alvarado, A. Regulation of Genomic Output and
1027 (Pluri)potency in Regeneration. *Annu. Rev. Genet.* **53**, 327-346, doi:10.1146/annurev-
1028 genet-112618-043733 (2019).

1029 69 McDonnell, E. *et al.* Lipids Reprogram Metabolism to Become a Major Carbon Source
1030 for Histone Acetylation. *Cell Rep* **17**, 1463-1472, doi:10.1016/j.celrep.2016.10.012
1031 (2016).

1032 70 Zhang, S. *et al.* A nuclear hormone receptor and lipid metabolism axis are required for
1033 the maintenance and regeneration of reproductive organs. *bioRxiv*, 279364,
1034 doi:10.1101/279364 (2018).

1035 71 Tsukada, Y. *et al.* Histone demethylation by a family of JmjC domain-containing proteins.
1036 *Nature* **439**, 811-816, doi:10.1038/nature04433 (2006).

1037 72 Robb, S. M. & Sánchez Alvarado, A. Histone modifications and regeneration in the
1038 planarian Schmidtea mediterranea. *Curr Top Dev Biol* **108**, 71-93, doi:10.1016/B978-0-
1039 12-391498-9.00004-8 (2014).

1040 73 Cao, P. L., Kumagai, N., Inoue, T., Agata, K. & Makino, T. JmjC Domain-Encoding
1041 Genes Are Conserved in Highly Regenerative Metazoans and Are Associated with
1042 Planarian Whole-Body Regeneration. *Genome Biol Evol* **11**, 552-564,
1043 doi:10.1093/gbe/evz021 (2019).

1044 74 Mihaylova, Y. *et al.* Conservation of epigenetic regulation by the MLL3/4 tumour
1045 suppressor in planarian pluripotent stem cells. *Nat Commun* **9**, 3633,
1046 doi:10.1038/s41467-018-06092-6 (2018).

1047 75 Hubert, A. *et al.* Epigenetic regulation of planarian stem cells by the SET1/MLL family of
1048 histone methyltransferases. *Epigenetics* **8**, 79-91, doi:10.4161/epi.23211 (2013).

1049 76 Mohamed Haroon, M. *et al.* Mitochondrial state determines functionally divergent stem
1050 cell population in planaria. *Stem Cell Reports*, doi:10.1016/j.stemcr.2021.03.022 (2021).

1051 77 Chung, S. *et al.* Mitochondrial oxidative metabolism is required for the cardiac
1052 differentiation of stem cells. *Nat. Clin. Pract. Cardiovasc. Med.* **4 Suppl 1**, S60-67,
1053 doi:10.1038/ncpcardio0766 (2007).

1054 78 Zhang, Y., Marsboom, G., Toth, P. T. & Rehman, J. Mitochondrial respiration regulates
1055 adipogenic differentiation of human mesenchymal stem cells. *PLoS One* **8**, e77077,
1056 doi:10.1371/journal.pone.0077077 (2013).

1057 79 Teixeira, F. K. *et al.* ATP synthase promotes germ cell differentiation independent of
1058 oxidative phosphorylation. *Nat. Cell Biol.* **17**, 689-696, doi:10.1038/ncb3165 (2015).

1059 80 Baris, O. R. *et al.* The mitochondrial electron transport chain is dispensable for
1060 proliferation and differentiation of epidermal progenitor cells. *Stem Cells* **29**, 1459-1468,
1061 doi:10.1002/stem.695 (2011).

1062 81 Panáková, D., Sprong, H., Marois, E., Thiele, C. & Eaton, S. Lipoprotein particles are
1063 required for Hedgehog and Wingless signalling. *Nature* **435**, 58-65,
1064 doi:10.1038/nature03504 (2005).

1065 82 Blomhoff, R. & Blomhoff, H. K. Overview of retinoid metabolism and function. *J.*
1066 *Neurobiol.* **66**, 606-630, doi:10.1002/neu.20242 (2006).

1067 83 Rigotti, A. Absorption, transport, and tissue delivery of vitamin E. *Mol Aspects Med* **28**,
1068 423-436, doi:10.1016/j.mam.2007.01.002 (2007).

1069 84 Gil, A., Plaza-Diaz, J. & Mesa, M. D. Vitamin D: Classic and Novel Actions. *Ann Nutr*
1070 *Metab* **72**, 87-95, doi:10.1159/000486536 (2018).

1071 85 Fernández-Barral, A. *et al.* Vitamin D differentially regulates colon stem cells in patient-
1072 derived normal and tumor organoids. *FEBS J.* **287**, 53-72, doi:10.1111/febs.14998
1073 (2020).

1074 86 Deng, S. *et al.* Vitamin E isomer delta-tocopherol enhances the efficiency of neural stem
1075 cell differentiation via L-type calcium channel. *Neurosci. Lett.* **585**, 166-170,
1076 doi:10.1016/j.neulet.2014.11.031 (2015).

1077 87 Gudas, L. J. & Wagner, J. A. Retinoids regulate stem cell differentiation. *J Cell Physiol*
1078 **226**, 322-330, doi:10.1002/jcp.22417 (2011).

1079 88 Lindsay-Mosher, N., Chan, A. & Pearson, B. J. Planarian EGF repeat-containing genes
1080 megf6 and hemicentin are required to restrict the stem cell compartment. *PLoS Genet.*
1081 **16**, e1008613, doi:10.1371/journal.pgen.1008613 (2020).

1082 89 Cote, L. E., Simental, E. & Reddien, P. W. Muscle functions as a connective tissue and
1083 source of extracellular matrix in planarians. *Nat Commun* **10**, 1592, doi:10.1038/s41467-
1084 019-09539-6 (2019).

1085 90 Betchaku, T. Isolation of planarian neoblasts and their behavior in vitro with some
1086 aspects of the mechanism of the formation of regeneration blastema. *J Exp Zool* **164**,
1087 407-433, doi:10.1002/jez.1401640310 (1967).

1088 91 Cruz, A. L. S., Barreto, E. A., Fazolini, N. P. B., Viola, J. P. B. & Bozza, P. T. Lipid
1089 droplets: platforms with multiple functions in cancer hallmarks. *Cell Death Dis* **11**, 105,
1090 doi:10.1038/s41419-020-2297-3 (2020).

1091 92 Tirinato, L. *et al.* An Overview of Lipid Droplets in Cancer and Cancer Stem Cells. *Stem*
1092 *Cells Int* **2017**, 1656053, doi:10.1155/2017/1656053 (2017).

1093 93 Sinclair, J. W. *et al.* A metabolic shift to glycolysis promotes zebrafish tail regeneration
1094 through TGF–β dependent dedifferentiation of notochord cells to form the blastema.
1095 *bioRxiv*, 2020.2003.2003.975318, doi:10.1101/2020.03.03.975318 (2020).

1096 94 Love, N. R., Ziegler, M., Chen, Y. & Amaya, E. Carbohydrate metabolism during
1097 vertebrate appendage regeneration: what is its role? How is it regulated?: A postulation
1098 that regenerating vertebrate appendages facilitate glycolytic and pentose phosphate

1099 pathways to fuel macromolecule biosynthesis. *Bioessays* **36**, 27-33,
1100 doi:10.1002/bies.201300110 (2014).

1101 95 Shyh-Chang, N., Daley, G. Q. & Cantley, L. C. Stem cell metabolism in tissue
1102 development and aging. *Development* **140**, 2535-2547, doi:10.1242/dev.091777 (2013).

1103 96 Olson, R. E. Discovery of the lipoproteins, their role in fat transport and their significance
1104 as risk factors. *J Nutr Sci* **128**, 439S-443S, doi:10.1093/jn/128.2.439S (1998).

1105 97 Feng, Y. *et al.* Hematopoietic stem/progenitor cell proliferation and differentiation is
1106 differentially regulated by high-density and low-density lipoproteins in mice. *PLoS One* **7**,
1107 e47286, doi:10.1371/journal.pone.0047286 (2012).

1108 98 Xu, J. *et al.* High density lipoprotein cholesterol promotes the proliferation of bone-
1109 derived mesenchymal stem cells via binding scavenger receptor-B type I and activation
1110 of PI3K/Akt, MAPK/ERK1/2 pathways. *Mol. Cell. Biochem.* **371**, 55-64,
1111 doi:10.1007/s11010-012-1422-8 (2012).

1112 99 Shen, H. *et al.* High density lipoprotein promotes proliferation of adipose-derived stem
1113 cells via S1P1 receptor and Akt, ERK1/2 signal pathways. *Stem Cell Res Ther* **6**, 95,
1114 doi:10.1186/s13287-015-0090-5 (2015).

1115 100 Safina, D. *et al.* Low-density lipoprotein receptor-related protein 1 is a novel modulator of
1116 radial glia stem cell proliferation, survival, and differentiation. *Glia* **64**, 1363-1380,
1117 doi:10.1002/glia.23009 (2016).

1118 101 Gaudet, D., Drouin-Chartier, J. P. & Couture, P. Lipid Metabolism and Emerging Targets
1119 for Lipid-Lowering Therapy. *Can J Cardiol* **33**, 872-882, doi:10.1016/j.cjca.2016.12.019
1120 (2017).

1121 102 Sánchez Alvarado, A., Newmark, P. A., Robb, S. M. & Juste, R. The *Schmidtea*
1122 *mediterranea* database as a molecular resource for studying platyhelminthes, stem cells
1123 and regeneration. *Development* **129**, 5659-5665 (2002).

1124 103 Roberts-Galbraith, R. H. & Newmark, P. A. Follistatin antagonizes Activin signaling and
1125 acts with Notum to direct planarian head regeneration. *Proc Natl Acad Sci U S A* **110**,
1126 1363-1368, doi:10.1073/pnas.1214053110 (2013).

1127 104 Forsthoefel, D. J., Cejda, N. I., Khan, U. W. & Newmark, P. A. Cell-type diversity and
1128 regionalized gene expression in the planarian intestine. *Elife* **9**, doi:10.7554/eLife.52613
1129 (2020).

1130 105 Brandl, H. *et al.* PlanMine--a mineable resource of planarian biology and biodiversity.
1131 *Nucleic Acids Res.* **44**, D764-773, doi:10.1093/nar/gkv1148 (2016).

1132 106 Zayas, R. M. *et al.* The planarian *Schmidtea mediterranea* as a model for epigenetic
1133 germ cell specification: analysis of ESTs from the hermaphroditic strain. *Proc. Natl.*
1134 *Acad. Sci. USA* **102**, 18491-18496 (2005).

1135 107 Potter, S. C. *et al.* HMMER web server: 2018 update. *Nucleic Acids Res.* **46**, W200-
1136 W204, doi:10.1093/nar/gky448 (2018).

1137 108 Guindon, S. *et al.* New algorithms and methods to estimate maximum-likelihood
1138 phylogenies: assessing the performance of PhyML 3.0. *Syst. Biol.* **59**, 307-321,
1139 doi:10.1093/sysbio/syq010 (2010).

1140 109 Forsthoefel, D. J., Waters, F. A. & Newmark, P. A. Generation of cell type-specific
1141 monoclonal antibodies for the planarian and optimization of sample processing for
1142 immunolabeling. *BMC Dev. Biol.* **14**, 45, doi:10.1186/s12861-014-0045-6 (2014).

1143 110 King, R. S. & Newmark, P. A. *In situ* hybridization protocol for enhanced detection of
1144 gene expression in the planarian *Schmidtea mediterranea*. *BMC Dev. Biol.* **13**, 8,
1145 doi:10.1186/1471-213X-13-8 (2013).

1146 111 Ross, K. G. *et al.* Novel monoclonal antibodies to study tissue regeneration in
1147 planarians. *BMC Dev. Biol.* **15**, 2, doi:10.1186/s12861-014-0050-9 (2015).

1148 112 Folch, J. & Lees, M. Proteolipides, a new type of tissue lipoproteins; their isolation from
1149 brain. *J. Biol. Chem.* **191**, 807-817 (1951).

1150 113 Carten, J. D., Bradford, M. K. & Farber, S. A. Visualizing digestive organ morphology
1151 and function using differential fatty acid metabolism in live zebrafish. *Dev. Biol.* **360**, 276-
1152 285, doi:10.1016/j.ydbio.2011.09.010 (2011).

1153 114 Andrews, S. *FastQC: a quality control tool for high throughput sequence data.*,
1154 <http://www.bioinformatics.babraham.ac.uk/projects/fastqc> (2010).

1155 115 Langmead, B. & Salzberg, S. L. Fast gapped-read alignment with Bowtie 2. *Nat.*
1156 *Methods* **9**, 357-359, doi:10.1038/nmeth.1923 (2012).

1157 116 Liao, Y., Smyth, G. K. & Shi, W. The R package Rsubread is easier, faster, cheaper and
1158 better for alignment and quantification of RNA sequencing reads. *Nucleic Acids Res.* **47**,
1159 e47, doi:10.1093/nar/gkz114 (2019).

1160 117 Robinson, M. D., McCarthy, D. J. & Smyth, G. K. edgeR: a Bioconductor package for
1161 differential expression analysis of digital gene expression data. *Bioinformatics* **26**, 139-
1162 140, doi:10.1093/bioinformatics/btp616 (2010).

1163 118 Maere, S., Heymans, K. & Kuiper, M. BiNGO: a Cytoscape plugin to assess
1164 overrepresentation of gene ontology categories in biological networks. *Bioinformatics* **21**,
1165 3448-3449, doi:10.1093/bioinformatics/bti551 (2005).

1166 119 de Hoon, M. J., Imoto, S., Nolan, J. & Miyano, S. Open source clustering software.
1167 *Bioinformatics* **20**, 1453-1454, doi:10.1093/bioinformatics/bth078 (2004).

1168 120 Saldanha, A. J. Java Treeview--extensible visualization of microarray data.
1169 *Bioinformatics* **20**, 3246-3248, doi:10.1093/bioinformatics/bth349 (2004).

1170 121 Livak, K. J. & Schmittgen, T. D. Analysis of relative gene expression data using real-time
1171 quantitative PCR and the 2(-Delta Delta C(T)) Method. *Methods* **25**, 402-408,
1172 doi:10.1006/meth.2001.1262 (2001).

1173 122 Thi-Kim Vu, H. *et al.* Stem cells and fluid flow drive cyst formation in an invertebrate
1174 excretory organ. *Elife* **4**, doi:10.7554/eLife.07405 (2015).

1175 123 Scimone, M. L., Srivastava, M., Bell, G. W. & Reddien, P. W. A regulatory program for
1176 excretory system regeneration in planarians. *Development* **138**, 4387-4398,
1177 doi:10.1242/dev.068098 (2011).

1178 124 Tu, K. C. *et al.* Egr-5 is a post-mitotic regulator of planarian epidermal differentiation.
1179 *Elife* **4**, e10501, doi:10.7554/eLife.10501 (2015).

1180 125 Schneider, C. A., Rasband, W. S. & Eliceiri, K. W. NIH Image to ImageJ: 25 years of
1181 image analysis. *Nat. Methods* **9**, 671-675, doi:10.1038/nmeth.2089 (2012).

1182 126 L, S. & ISoMaM, S. GeneOverlap: Test and visualize gene overlaps. *R package version*
1183 *1.28.0* (2021). <https://bioconductor.org/packages/release/bioc/html/GeneOverlap.html>.
1184

1185

1186 **Figures and Figure Legends**

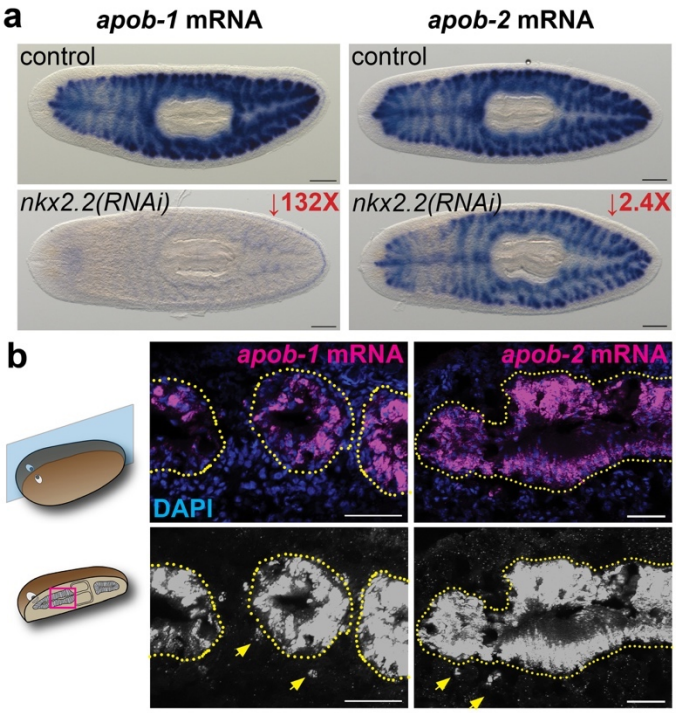

1187

1188 **Figure 1.**

1189 **Figure 1. Transcripts encoding planarian *apolipoprotein b* orthologs are intestine-**

1190 **enriched and downregulated in *nkx2.2(RNAi)* animals. (a)** *apob-1* and *apob-2* mRNA (ISH)

1191 expression in control (top) and *nkx2.2(RNAi)* planarians. **(b)** *apob-1* and *apob-2* mRNA

1192 expression (FISH) in sagittal sections. Arrows indicate *apob*-expressing cells (likely

1193 differentiating phagocytes) outside the intestine (dotted yellow outline) in digitally brightened

1194 images. Scale bars: 200 μm **(a)**; 50 μm **(b)**.

1195

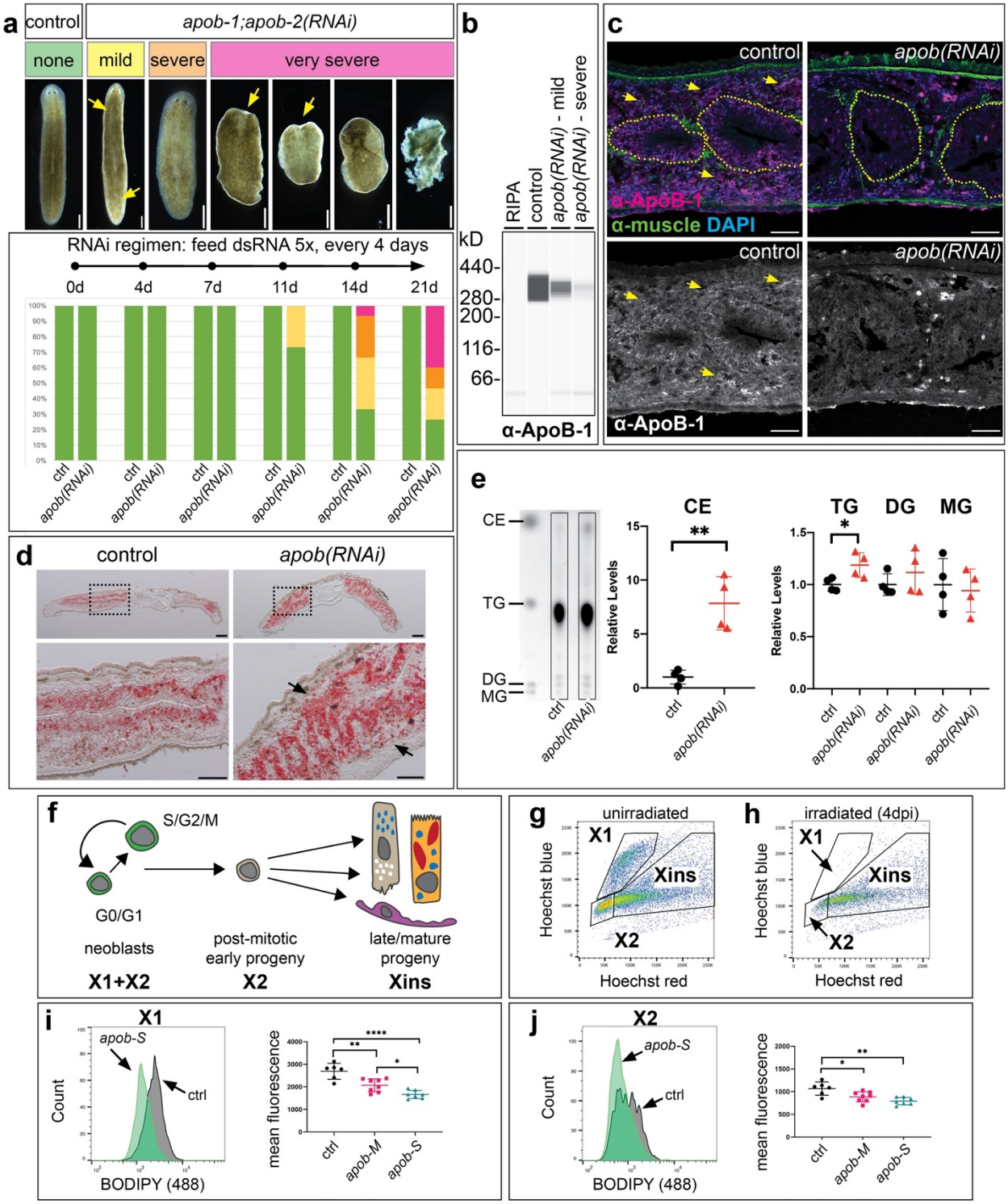

1196

1197

1198 **Figure 2.**

1199 **Figure 2. *apob* orthologs are required for viability and neutral lipid metabolism. (a)**
1200 Simultaneous RNAi-mediated knockdown of *apob-1* and *apob-2* caused mild (yellow) and
1201 severe (orange) depigmentation, and very severe (pink) phenotypes including head regression,
1202 ventral curling, and lysis. Knockdown was initiated with n = 15 animals per condition. **(b)** Simple
1203 Western (capillary-based protein analysis) lane view of extracts from control and knockdown
1204 planarians labeled with custom anti-ApoB-1. **(c)** ApoB-1 protein expression in sagittal sections.
1205 Expression in intestine (dotted outline) and outside the intestine (arrows) was dramatically
1206 reduced in "very severe" *apob-1(RNAi);apob-2(RNAi)* planarians (right panels). mAb 6G10
1207 (green) labeled body wall, dorsoventral, and visceral muscle fibers (demarcating the intestine.)
1208 **(d)** Neutral lipids accumulated in the intestine and parenchyma (arrows) of "mild" *apob(RNAi)*
1209 planarians. Oil Red O labeling, sagittal sections. **(e)** Cholesteryl esters (CE) and triglycerides
1210 (TG), but not diacylglycerides (DG) or monoglycerides (MG) were significantly elevated in "mild"
1211 *apob(RNAi)* animals. Thin layer chromatography, intensities of lipid species measured in
1212 ImageJ and normalized to controls. Student's t test (unpaired, two-tailed); p=.0017 (CE) and
1213 p=.0303 (TG). Error bars: mean ± S.D., n=4. **(f)** Lineage schematic indicating cell types in X1,
1214 X2, and Xins subpopulations. **(g)** Example flow plot for uninjured animals. **(h)** Example plot for
1215 animals 4 days post irradiation ("4 dpi"), showing ablation of cells in X1 and depletion of cells in
1216 X2. **(i-j)** *apob* knockdown caused reduction of neutral lipids in X1 and X2 cells. One-way
1217 ANOVA with Tukey's multiple comparisons test. Error bars: mean ± S.D., n≥6 biological
1218 replicates per condition. Scale bars: 50 µm **(c)**; 200 µm **(d,** upper panels**)**; 100 µm **(d,** lower
1219 panels**)**.
1220

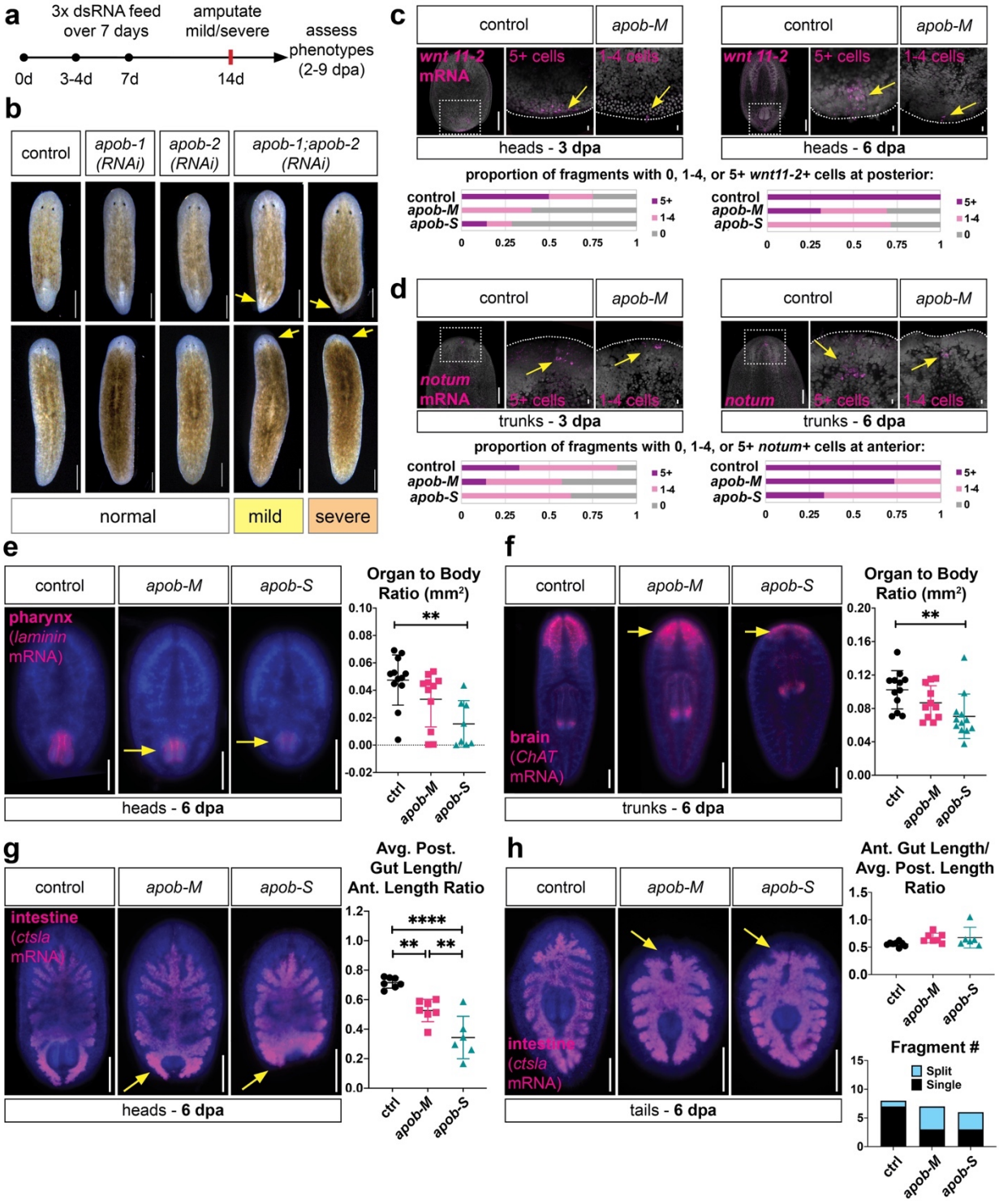
a
3x dsRNA feed over 7 days
amputate mild/severe
assess phenotypes (2-9 dpa)
0d
3-4d
7d
14d
b
control
apob-1 (RNAi)
apob-2 (RNAi)
apob-1;apob-2 (RNAi)
normal
mild
severe
c
control
apob-M
wnt 11-2 mRNA
5+ cells
1-4 cells
heads - 3 dpa
heads - 6 dpa
proportion of fragments with 0, 1-4, or 5+ wnt11-2+ cells at posterior:
control
apob-M
apob-S
5+
1-4
0
d
notum mRNA
trunks - 3 dpa
trunks - 6 dpa
proportion of fragments with 0, 1-4, or 5+ notum+ cells at anterior:
e
apob-S
pharynx (laminin mRNA)
heads - 6 dpa
Organ to Body Ratio (mm²)
ctrl
f
brain (ChAT mRNA)
trunks - 6 dpa
g
intestine (ctsla mRNA)
Avg. Post. Gut Length/ Ant. Length Ratio
h
tails - 6 dpa
Ant. Gut Length/ Avg. Post. Length Ratio
Fragment #
Split
Single

Figure 3.

1224 **Figure 3. *apob* inhibition delays regeneration. (a)** Schematic of RNAi treatment and analysis
1225 regimen. **(b)** *apob* double knockdown resulted in smaller blastemas (arrows) in head and trunk
1226 regenerates (8 dpa). **(c-d)** Differentiation of cells expressing polarity genes *wnt11-2* (posterior)
1227 and *notum* (anterior) was delayed in *apob(RNAi) animals.* FISH; max projections of confocal
1228 images. n=5-15 fragments per condition were scored for number of positive cells. Control and
1229 *apob-M* fragments shown as phenotype examples. **(e)** Pharynx regeneration was reduced in
1230 *apob(RNAi)* head regenerates (6 dpa) (*laminin* mRNA FISH, epifluorescent images). p=.0021,
1231 control vs. *apob-S.* **(f)** CNS regeneration was reduced in *apob(RNAi)* tail regenerates (6 dpa)
1232 (*ChAT* mRNA FISH, epifluorescent images). p=.0101, control vs. *apob-S.* **(g-h)** *apob* RNAi
1233 disrupted intestine regeneration (6 dpa) (*ctsla* mRNA FISH, epifluorescent images). New
1234 branches were shorter in heads **(g)**. p=.0004 (*apob-M*); p=.0016 (*apob-S*). New branches often
1235 failed to fuse in tails **(h)**. Significance testing in **(e-h)**: one-way ANOVA with Tukey's multiple
1236 comparisons test. Error bars: mean +/- S.D., n≥7 per condition. DAPI (blue) in **(e-h)**. Scale bars:
1237 500 µm **(b)**; 200 µm **(c-d);** 10 µm **(c-d** insets**);** 200 µm **(e-h)**.
1238

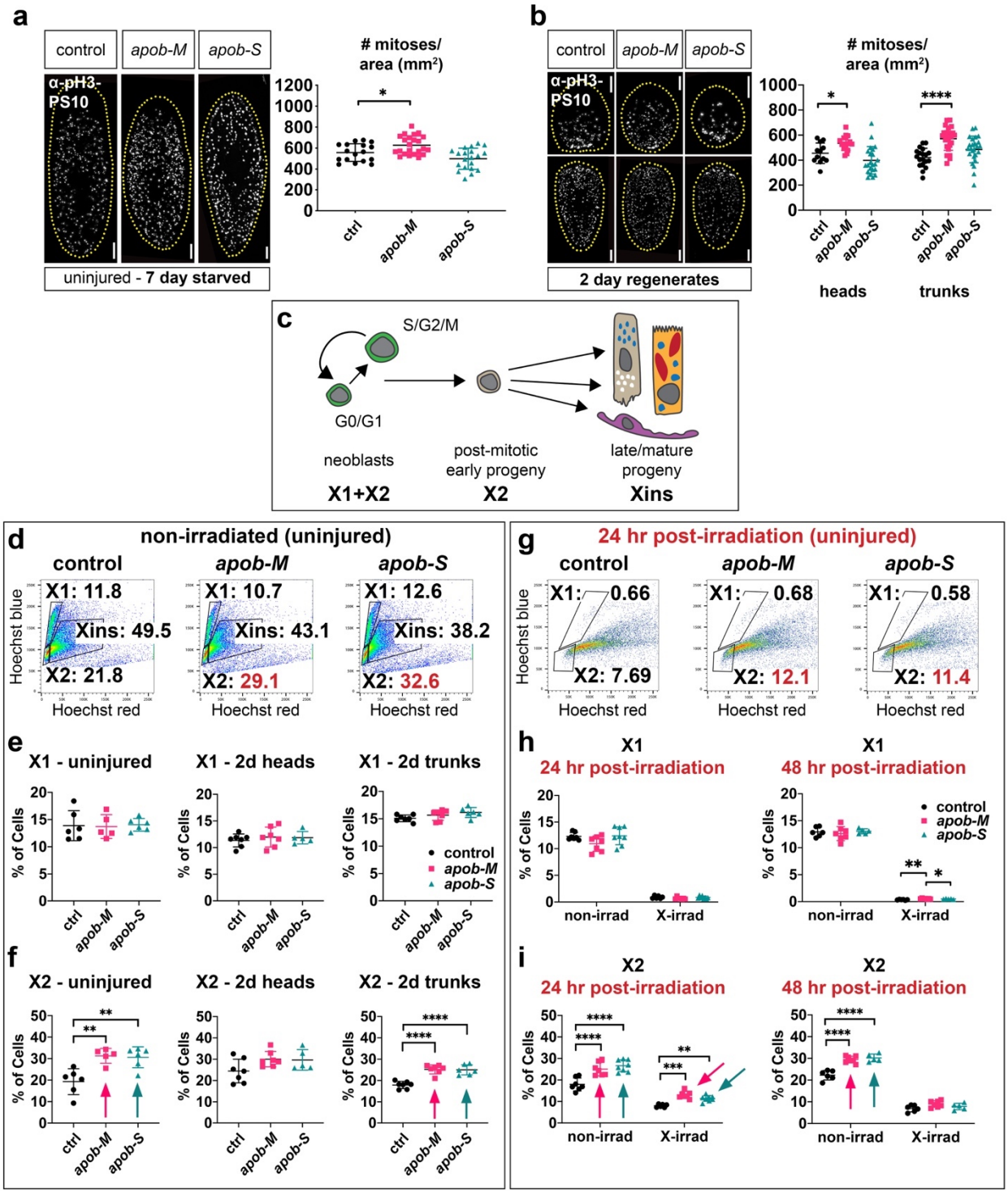
a
control
apob-M
apob-S
α-pH3-PS10
uninjured - 7 day starved
mitoses/ area (mm²)
ctrl
apob-M
apob-S
b
2 day regenerates
heads
trunks
c
S/G2/M
G0/G1
neoblasts
X1+X2
post-mitotic early progeny
X2
late/mature progeny
Xins
d
non-irradiated (uninjured)
Hoechst blue
Hoechst red
X1: 11.8
Xins: 49.5
X2: 21.8
X1: 10.7
Xins: 43.1
X2: 29.1
X1: 12.6
Xins: 38.2
X2: 32.6
e
X1 - uninjured
X1 - 2d heads
X1 - 2d trunks
% of Cells
f
X2 - uninjured
X2 - 2d heads
X2 - 2d trunks
g
24 hr post-irradiation (uninjured)
X1: 0.66
X2: 7.69
X1: 0.68
X2: 12.1
X1: 0.58
X2: 11.4
h
X1
24 hr post-irradiation
48 hr post-irradiation
non-irrad
X-irrad
i
X2

Figure 4.

1242 **Figure 4. *apob* inhibition causes accumulation of neoblast progeny. (a-b)** PhosphoHistone-
1243 H3-S10-positive (pH3-PS10) cells were modestly elevated in *apob-M,* but not *apob-S,* uninjured
1244 animals **(a)** and 2-day regenerates **(b)**. One-way ANOVA with Dunnett's T3 multiple
1245 comparisons test. Error bars: mean +/- S.D., n≥12 animals/fragments per condition **(a-b)**. **(c)**
1246 Lineage schematic indicating cell types/states in X1, X2, and Xins subpopulations. **(d)** Examples
1247 of flow dot plots from uninjured planarians indicating percentages of cells in each gate, with X2
1248 increase in *apob(RNAi)* animals in red. **(e-f)** Percentage of cells in X1 **(e)** and X2 **(f)** in uninjured
1249 (left), 2-day head (middle), and 2-day trunk (right) regenerates. Arrows indicate statistically
1250 significant increases in X2. **(g)** Examples of flow plots from uninjured planarians, 24 hr post-
1251 irradiation, indicating percentages of cells in each gate, with X2 increase in *apob(RNAi)* animals
1252 in red. **(h-i)** Percentage of cells in X1 **(h)** and X2 **(i)** in uninjured planarians, 24 hr (left) and 48 hr
1253 (right) post-irradiation. Arrows indicate significant increases in X2. One-way ANOVA and
1254 Tukey's multiple comparisons test for non-irradiated samples and X1 irradiated samples (*p*
1255 values in **e-f, h**, see Methods). Two-way ANOVA and two-stage linear step-up procedure of
1256 Benjamini, Krieger and Yekutieli for multiple comparisons for X2 irradiated samples (*q* values in
1257 **i**). Although differences between RNAi conditions in X1 at 48 hr post-irradiation were significant,
1258 percent of cells in this gate was negligible (<0.7% in all samples). Error bars = mean ± S.D, n≥5
1259 biological replicates per condition. Scale bars: 200 μm **(a-b)**.
1260

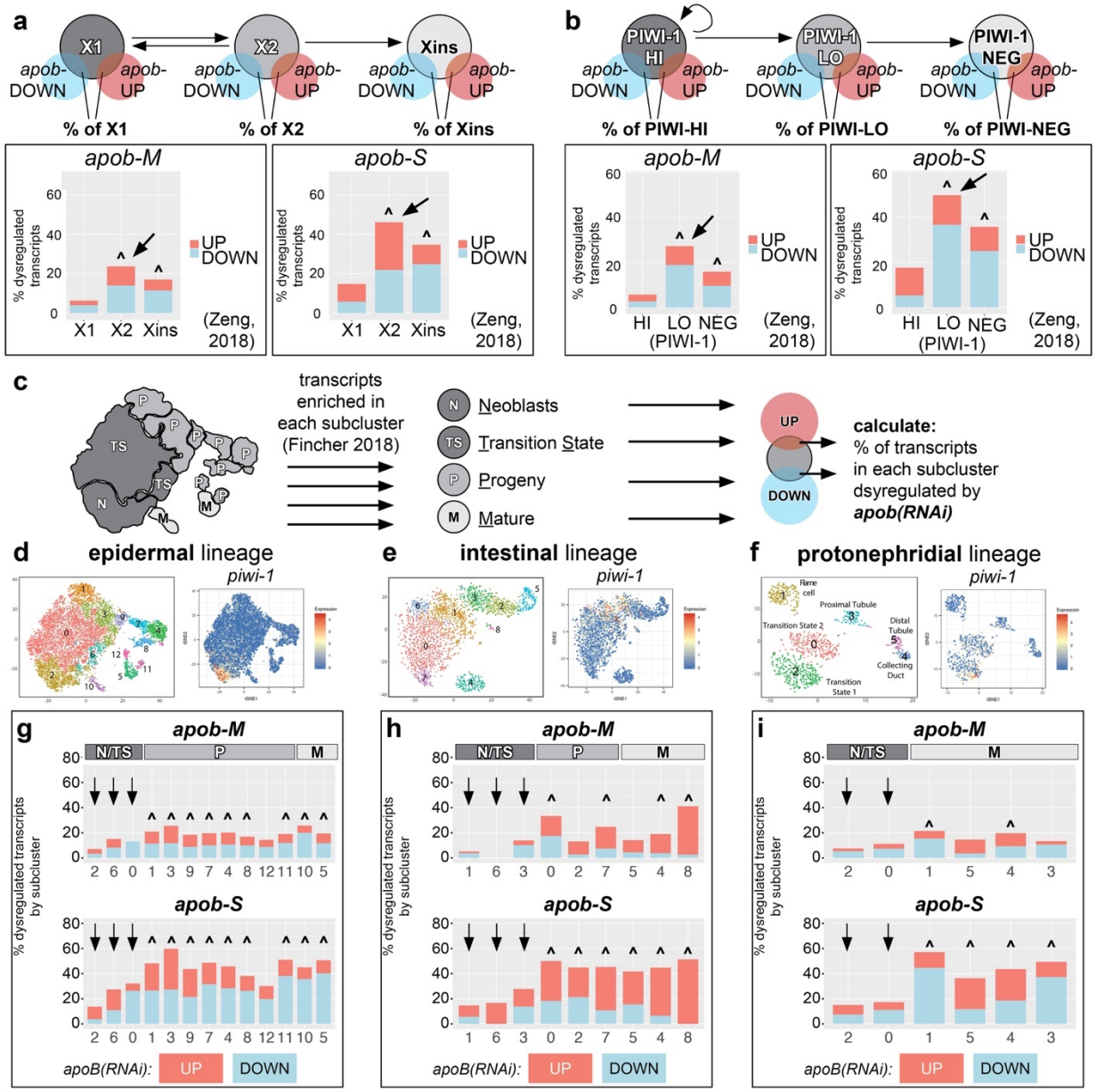

1261

1262

1263 **Figure 5.**

1264 **Figure 5. *apob* RNAi preferentially dysregulates transcripts in differentiating neoblast**
1265 **progeny and mature cell states. (a-b)** *apob* RNAi dysregulates greater proportions of X2 **(a)**
1266 and PIWI-LO **(b)** signature transcripts (arrows in histograms). Venn diagrams at top show
1267 analysis scheme: percent of X1/X2/Xins **(a)** and PIWI-HI/PIWI-LO/PIWI-NEG **(b)** signature
1268 transcripts [49] that overlap with transcripts dysregulated in *apob-M/apob-S* animals (this study)
1269 (see also Supp. Fig. 6a-d). Histograms show percentage of signature transcripts up- and down-
1270 regulated in *apob-M/apob-S* animals. **(c)** Schematic example (for epidermal lineage) illustrating
1271 how transcripts dysregulated in *apob(RNAi)* animals were cross-referenced with neoblast (N),
1272 transition state (TS), progeny (P), and mature (M) cell state subclusters from[40]. See Methods for
1273 details. **(d-f)** t-SNE plots (digiworm.wi.mit.edu) indicate subclusters and *piwi-1* mRNA
1274 expression for each lineage. **(g-i)** *apob* knockdown dysregulated greater proportions of
1275 transcripts enriched in progeny ("P") and mature ("M") cell subclusters in multiple cell type
1276 lineages. Arrows indicate less-affected transcripts enriched in neoblasts/transition state ("N/TS")
1277 subclusters. Carets (^) **(a, b, g-i)** indicate significant gene expression overlap ($p<0.05$, Fisher's
1278 exact test, see Source Data 2 for individual p values).
1279

1280

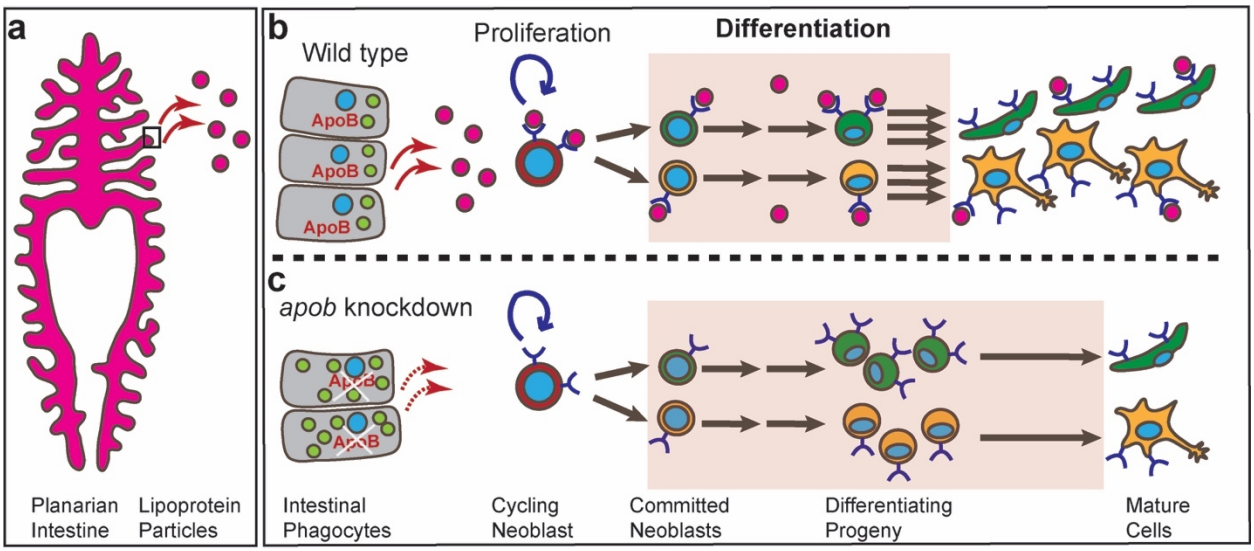

1281

1282 **Figure 6.**

1283

1284 **Figure 6. A putative model for ApoB function in regulating differentiation of planarian**
1285 **stem cell progeny. (a)** Our data support a working model in which ApoB is expressed by
1286 phagocytes in the intestine, a primary site of LP production and secretion. **(b)** ApoB mediates
1287 secretion of neutral lipids in LPs from intestinal phagocytes to neoblasts and their progeny. **(c)**
1288 In the absence of ApoB, lipids accumulate in the intestine, and LP delivery to neoblasts and
1289 their progeny is disrupted, reducing their neutral lipid content. Neoblast proliferation and renewal
1290 are largely unaffected by reduced ApoB function. Instead, differentiation and later maturation of
1291 most, if not all, planarian cell lineages are slowed, causing an accumulation of differentiating
1292 progeny and a delay in regeneration of multiple organs. Box in **(a)** represents region magnified
1293 in **(b)** wild type and **(c)** *apob* knockdown conditions. Nuclei, blue. Lipid droplets, light green.
1294 LPs, magenta. Apical/lumenal phagocyte surface is to the left and basal/mesenchymal
1295 phagocyte surface is to the right in **(b, c)**.
1296

Supplementary Figures and Figure Legends

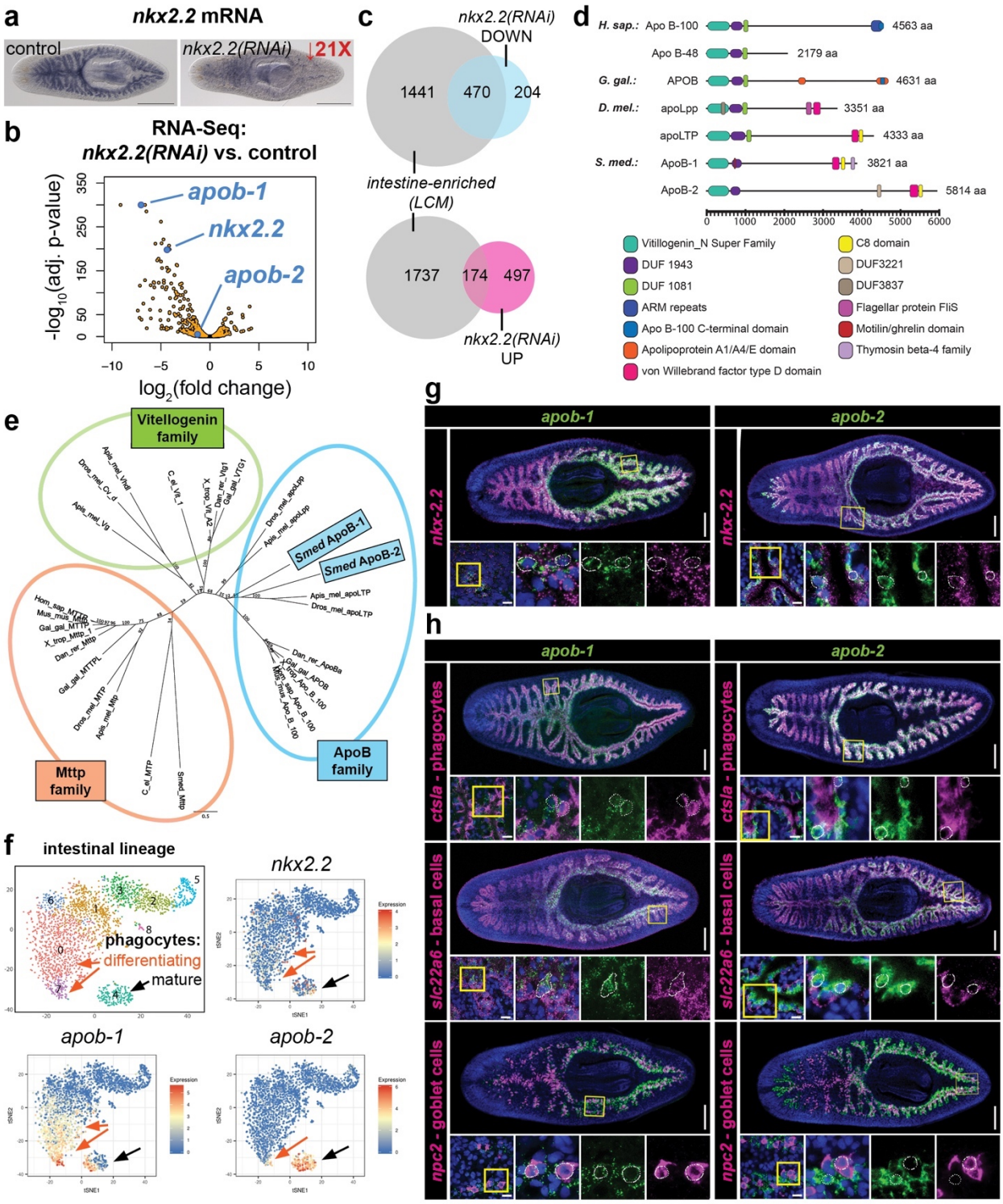

Supplementary Figure 1.

1300 **Supplementary Figure 1. *apob-1* and *apob-2* encode intestine-enriched ApoB orthologs.**
1301 **(a)** *nkx2.2* mRNA *in situ* expression patterns in uninjured control and *nkx2.2(RNAi)* planarians.
1302 **(b)** Volcano plot showing downregulation of *apob-1, apob-2,* and *nkx2.2* in *nkx2.2(RNAi)*
1303 animals. An offset of 1e-300 was added to all FDR-adjusted *p* values to enable plotting of
1304 transcripts with *p*=0. **(c)** 470 downregulated (top) and 174 upregulated (bottom) transcripts in
1305 *nkx2.2(RNAi)* animals exhibited intestine enrichment in a previous study[104]. Total numbers of
1306 dysregulated transcripts in *nkx2.2(RNAi)* samples were slightly lower than in Supplementary
1307 Data 1, because some were undetectable in the intestine data set. **(d)** Conserved domains in
1308 human (*H. sap.),* chicken (*G. gal.*), fly (*D. mel.*), and planarian (*S. med.*) ApoB proteins. **(e)**
1309 Phylogenetic relationship of planarian (*Smed*) ApoB-1 and ApoB-2 (based on similarity of N-
1310 terminal Vitellogenin domains) with closely related protein families in human (*Hom_sap*), mouse
1311 (*Mus_mus*), chicken (*Gal_gal*), fly (*Dros_mel*), honeybee (*Apis_mel*), frog (*X_trop*), and *C.*
1312 *elegans* (*C_el*). Branch support is indicated. **(f)** t-SNE plots from single cell transcriptomes[40]
1313 showing expression of *nkx2.2, apob-1,* and *apob-2* in the intestinal lineage. All transcripts were
1314 enriched in differentiating progeny (subclusters 0/7, orange arrows) and mature phagocytes
1315 (subcluster 4, black arrow); *nkx2.2* was also enriched in neoblasts/transition state cells
1316 (subcluster 1). **(g)** Double FISH showing co-expression of *apob-1, apob-2,* and *nkx2.2* mRNA.
1317 **(h)** Double FISH showing expression of *apob-1, apob-2* in phagocytes and basal cells (*apob-1*
1318 only), but not goblet cells. Yellow boxes indicate regions magnified in insets. Scale bars: 500 μm
1319 **(a)**; 200 μm **(g-h)**; 10 μm **(g-h** insets, bottom left**).**
1320

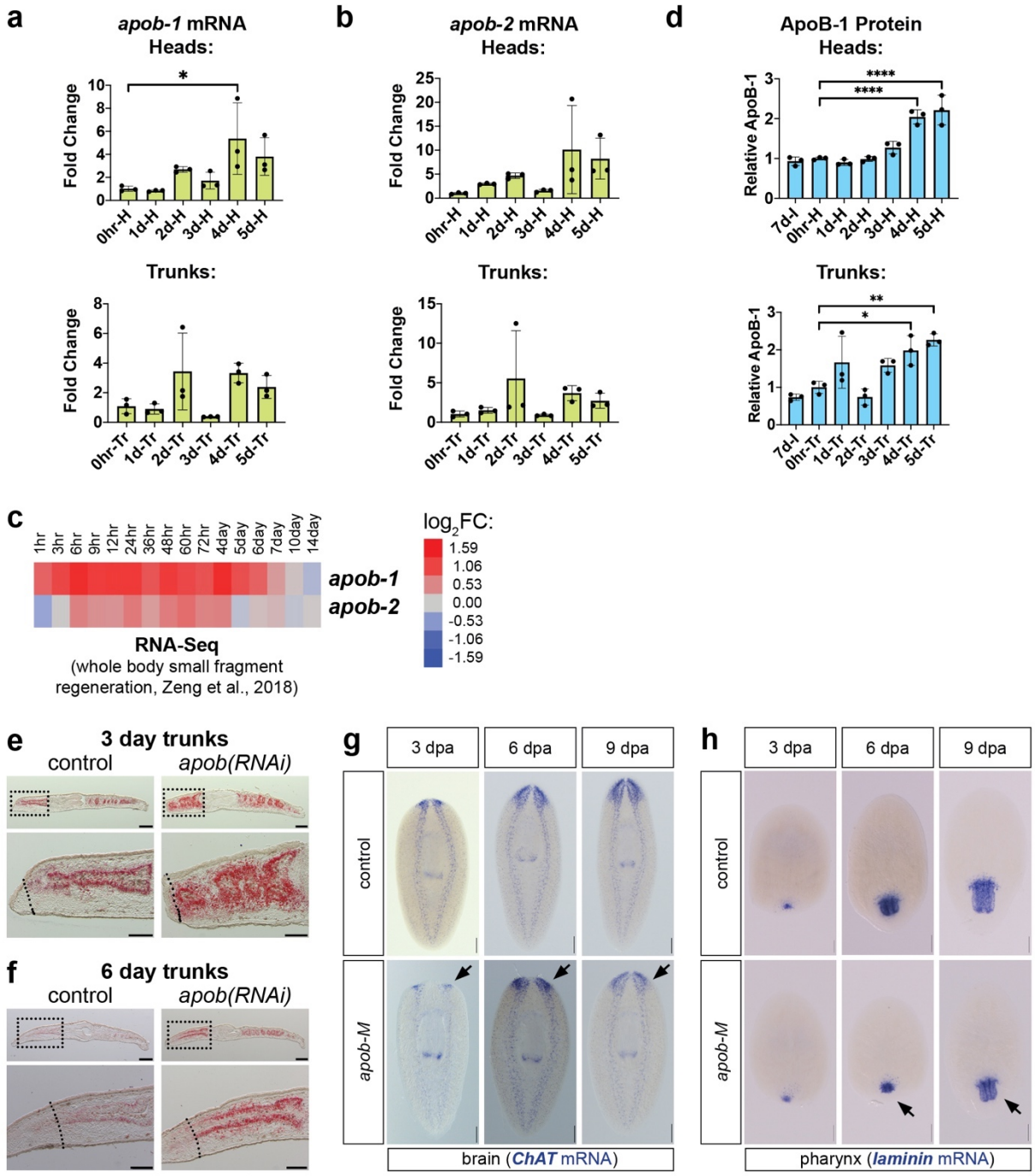

Supplementary Figure 2.

1324 **Supplementary Figure 2. Further characterization of *apob* expression and RNAi**
1325 **phenotypes. (a)** *apob-1* mRNA was upregulated in head and trunk regenerates (qRT-PCR). **(b)**
1326 *apob-2* mRNA was upregulated in head and trunk regenerates (qRT-PCR). **(c)** *apob-1* and
1327 *apob-2* mRNA levels were upregulated in whole fragment regeneration RNA-Seq data (Zeng et
1328 al., 2018). **(d)** ApoB-1 protein was upregulated during regeneration (3-5 dpa) in head and trunk
1329 fragments (Simple Western "Wes" capillary-based immunoassay). 7d-I, 7 day Intact (starved
1330 and uninjured) animals. **(e-f)** Neutral lipids accumulate in *apob*(RNAi) ("mild") regenerates.
1331 Dashed line indicates approximate plane of amputation. Anterior is left. **(g-h)** Brain (G) and
1332 pharynx (H) regeneration were delayed, but not blocked, by *apob* RNAi. Arrows indicate smaller
1333 organs in *apob-M* animals relative to controls (representative images). Significance testing
1334 (qPCR and Wes): one-way ANOVA (comparisons to 0 hr controls) with Dunnett's T3 multiple
1335 comparisons test. Error bars = mean +/- S.D. DAPI (blue) in **(d-g)**. Scale bars: 200 μm **(e-f,**
1336 upper panels**)**; 100 μm **(e-f,** lower panels**)**; 100 μm **(g-h)**.
1337

1338

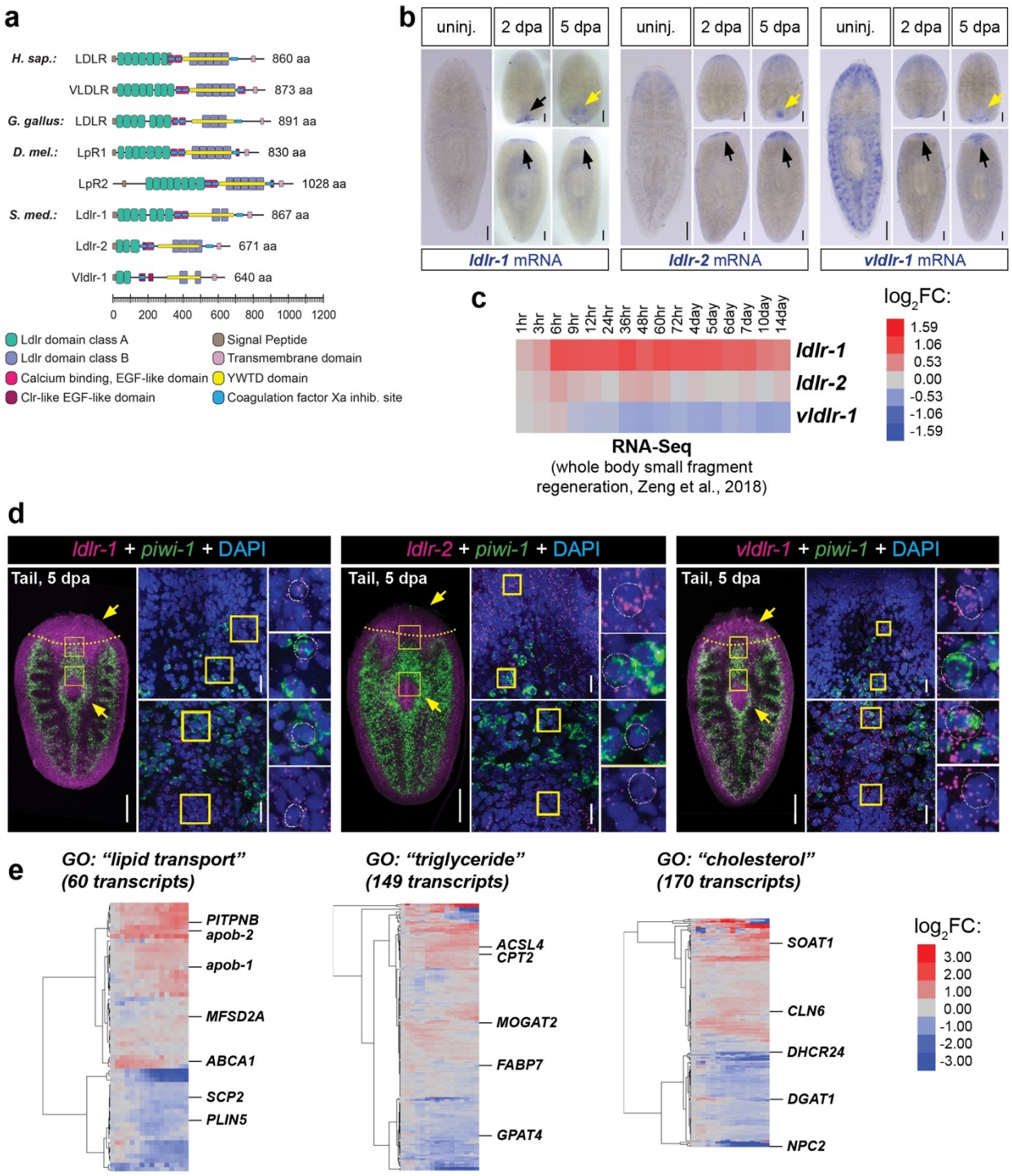

1339

1340 **Supplementary Figure 3.**

1341 **Supplementary Figure 3. Lipoprotein receptor expression is upregulated during planarian**
1342 **regeneration. (a)** Schematic of domains in LDLR and related homologs. Only domains common
1343 to Ldlr-like proteins in multiple species are shown. Clr-like EGF-like domains are shown only if
1344 they do not overlap with Ca-binding EGF-like domains. **(b)** WISH showing upregulation of
1345 planarian *ldlr* homologs in blastemas (black arrows) or developing pharynges (yellow arrows) at
1346 2 and 5 dpa. **(c)** *ldlr-1* and *ldlr-2* mRNA levels were upregulated in whole fragment regeneration
1347 RNA-Seq data (Zeng et al., 2018). **(d)** *ldlr* homologs (magenta, mRNA FISH) were expressed in
1348 *piwi-1*+ neoblasts (green, mRNA FISH) as well as differentiating (*piwi-1*-negative*)* cells in brain
1349 and pharynx (arrows) in 5-day regenerates. **(e)** Heat maps showing numerous planarian
1350 transcripts related to lipid metabolism that were up- and down-regulated during regeneration in
1351 whole fragment regeneration RNA-Seq data (Zeng et al., 2018). See Supplementary Data 3 for
1352 transcript IDs and expression data. Scale bars: 200 μm **(b)**; 200 μm **(d,** left panels**)**; 20 μm **(d,**
1353 right panels**)**.
1354

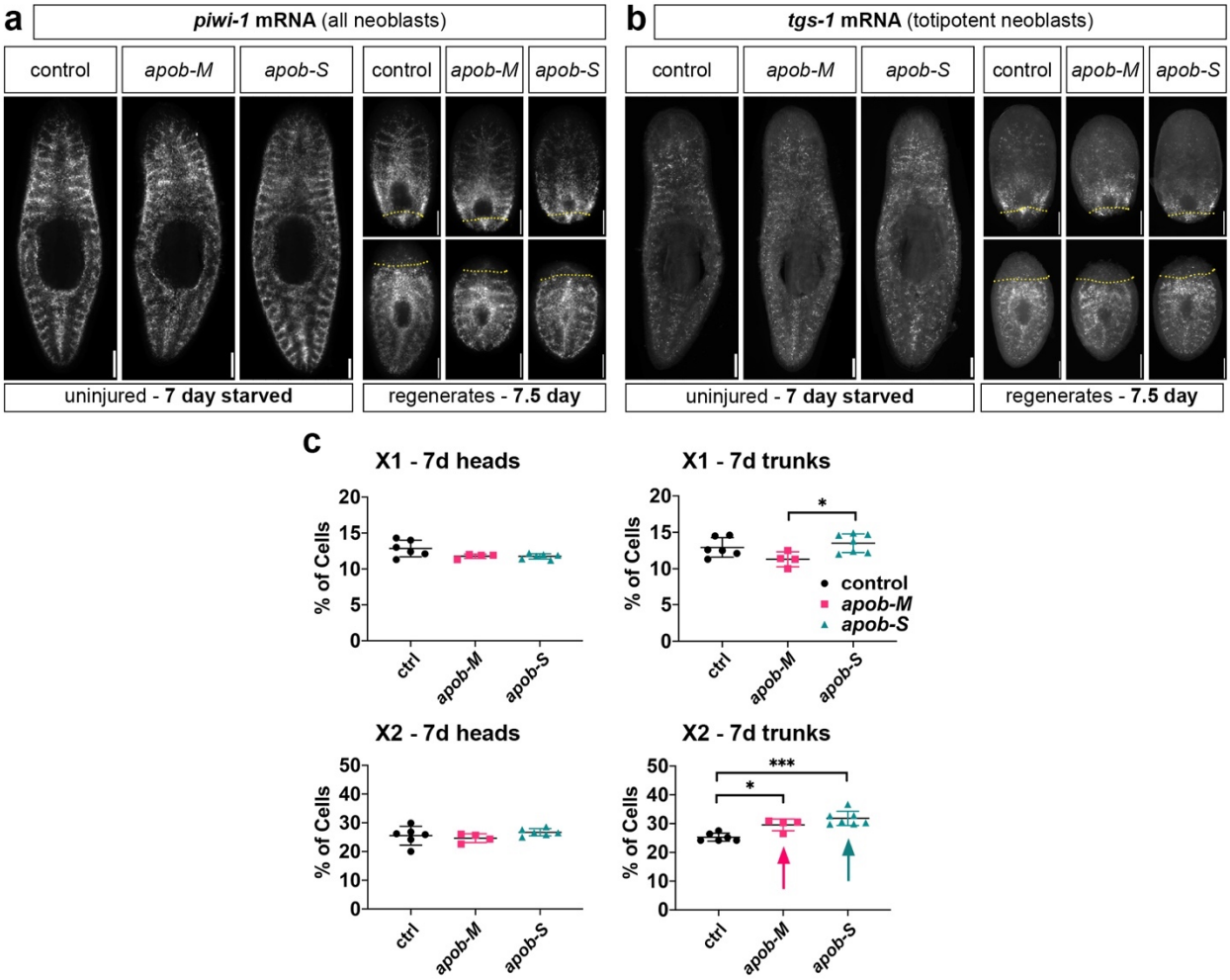

Supplementary Figure 4.

1358 **Supplementary Figure 4. Further characterization of effects of *apob* inhibition on**
1359 **neoblasts and neoblast progeny. (a)** Distribution of *piwi-1*-expressing neoblasts in uninjured
1360 (7 day starved, left panels) and 7.5 dpa head and tail regenerates (right panels). **(b)** Distribution
1361 of *tgs-1*-expressing neoblasts in uninjured (7 day starved, left panels) and 7.5 dpa head and tail
1362 regenerates (right panels). Whole-mount FISH **(a, b)**; epifluorescent images of representative
1363 samples. Dotted lines, approximate amputation plane. **(c)** Percentage of cells in X1 and X2 in 7
1364 day head (left) and trunk (right) regenerates. Arrows indicate significant increases in X2. One-
1365 way ANOVA and Dunnett's (X1, 7 day heads) or Tukey's (all others) multiple comparisons test.
1366 Error bars = mean +/- S.D. Scale bars: 200 μm **(a-b)**.
1367

1368

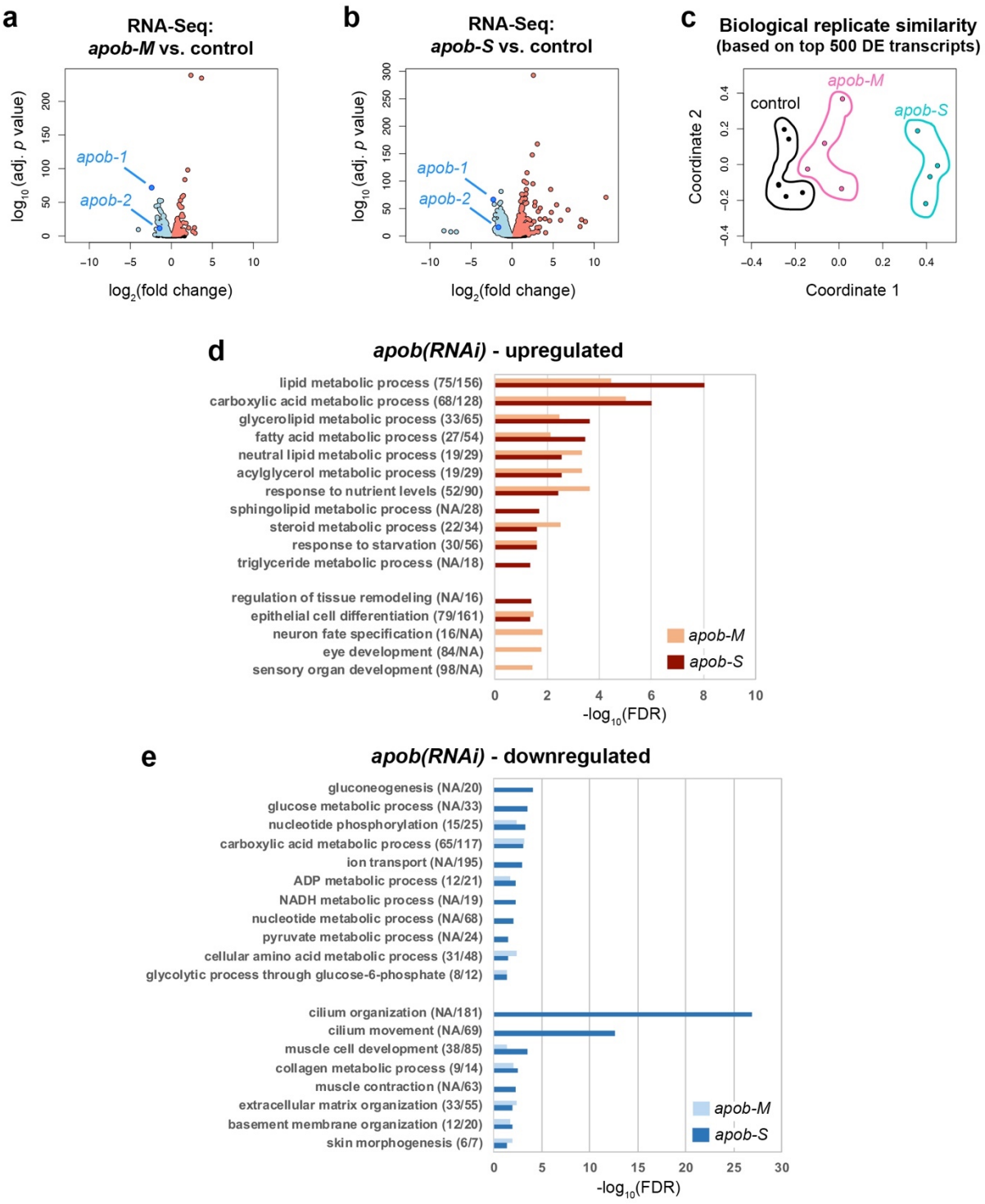

1369

1370 **Supplementary Figure 5.**

1371 **Supplementary Figure 5. *apob* RNAi dysregulates transcripts involved in metabolism-**
1372 **and differentiation-related processes. (a-b)** Volcano plots showing significantly
1373 downregulated (blue) and upregulated (pink) transcripts in *apob-M* **(a)** and *apob-S* **(b)** uninjured
1374 animals. **(c)** Multi-dimensional scaling plot showing similarity of control and RNAi sample
1375 libraries, using the biological coefficient of variation method to calculate distances between each
1376 library based on the 500 most variable transcripts across all samples. **(d-e)** Gene Ontology
1377 Biological Process categories over-represented among transcripts upregulated **(d)** or
1378 downregulated **(e)** by *apob* RNAi. Numbers of transcripts dysregulated indicated in parentheses
1379 (*apob-M/apob-S*). NA, not applicable (GO category not enriched in *apob-M* or *apob-S*). -
1380 $\log_{10}$(FDR) on X-axis.
1381

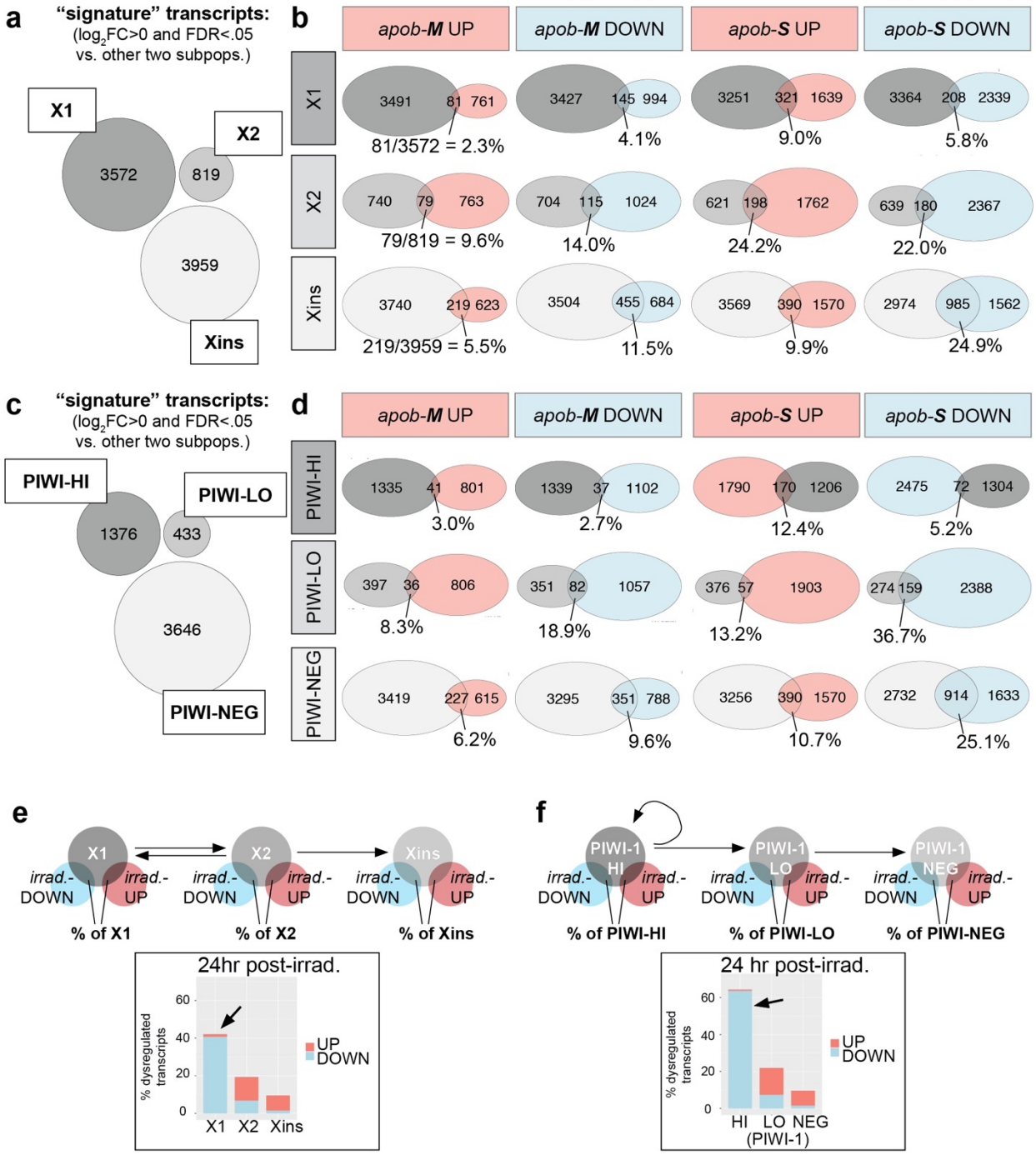

Supplementary Figure 6.

1385 **Supplementary Figure 6. *apob* RNAi preferentially dysregulates transcripts in**
1386 **differentiating neoblast progeny and mature post-mitotic cells. (a)** Venn diagram showing
1387 no overlap between X1, X2, and Xins "signature" transcripts (defined as having logFC>0
1388 (FDR<.05) vs. transcripts in both other fractions). **(b)** Venn diagrams showing overlap between
1389 X1, X2, and Xins signature transcripts and transcripts up or down in *apob-M* and *apob-S*.
1390 Percentages of X1/X2/Xins dysregulated are indicated. **(c)** Venn diagram showing no overlap
1391 between PIWI-HI, PIWI-LO, and PIWI-NEG signature transcripts (defined as having logFC>0
1392 (FDR<.05) vs. transcripts in both other fractions). **(d)** Venn diagrams showing overlap between
1393 PIWI-HI, PIWI-LO, and PIWI-NEG signature transcripts and transcripts up or down in *apob-M*
1394 and *apob-S*. Percentages of PIWI-HI/PIWI-LO/PIWI-NEG dysregulated are indicated. **(e-f)** X1-
1395 enriched **(e)** and PIWI-HI-enriched **(f)** signature transcripts were preferentially downregulated in
1396 planarians 24 hr post-irradiation. Venn diagrams at top show analysis schemes: percent of
1397 X1/X2/Xins **(e)** and PIWI-HI/PIWI-LO/PIWI-NEG **(f)** signature transcripts that overlap with
1398 transcripts dysregulated in planarians 24 hr post-irradiation. Histograms show percentage of
1399 signature transcripts up- and down-regulated in planarians 24 hr post-irradiation. Analysis of
1400 data from [49] (see Methods).
1401

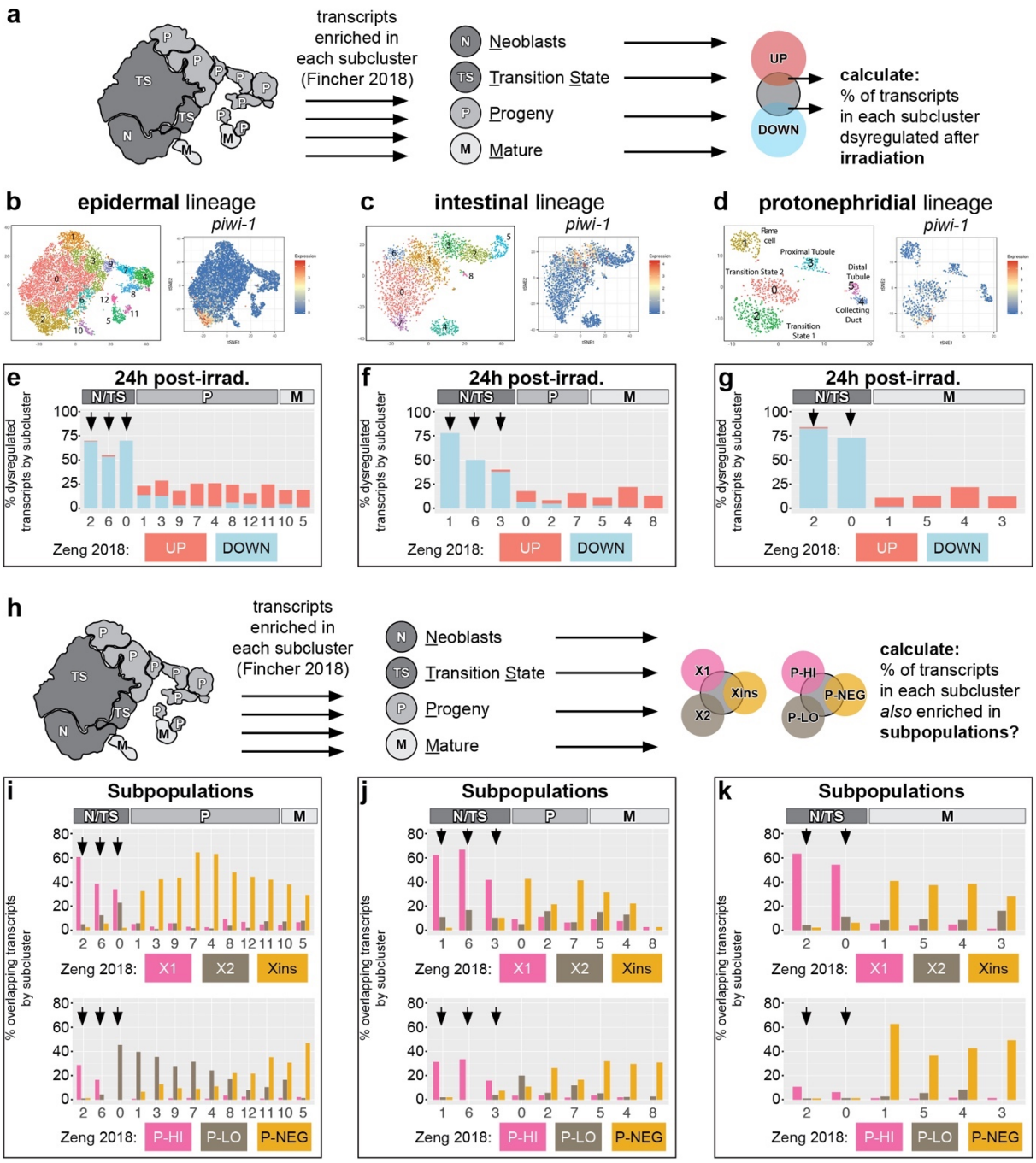

Supplementary Figure 7.

1405 **Supplementary Figure 7. Mapping of transcripts from 24 hr post-irradiation and cell-state-**
1406 **enriched subpopulations to single-cell subclusters in three lineages. (a)** Schematic
1407 example (for epidermal lineage) illustrating how transcripts dysregulated in 24 hr post-irradiation
1408 animals[49] were cross-referenced with neoblast (N), transition state (TS), progeny (P), and
1409 mature (M) cell state subclusters[40]. See Methods for details. **(b-d)** t-SNE plots
1410 (digiworm.wi.mit.edu) indicate subclusters and *piwi-1* mRNA expression for each lineage. **(e-g)**
1411 Cross-referencing of scRNA-Seq data[40] with RNA-Seq data from whole planarians 24 hr post-
1412 irradiation[49]. Histograms showing that irradiation preferentially caused downregulation of
1413 transcripts enriched in neoblast ("N") and transition state ("TS") subclusters in multiple cell type
1414 lineages (arrows), by contrast to the effects of *apob* RNAi (see also Fig. 5). **(h)** Cell state
1415 schematic and Venn diagrams show analysis strategy to calculate proportion of subcluster-
1416 enriched transcripts[40] also enriched in sorted planarian cell subpopulations[49]. **(i-k)** Cross-
1417 referencing of scRNA-Seq data[40] with bulk sorted cell RNA-Seq data[49]. Histograms showing that
1418 X1/PIWI-HI ("P-HI") signature transcripts were primarily enriched in neoblast ("N") and transition
1419 state ("TS") subclusters, and that Xins/PIWI-NEG ("P-NEG") signature transcripts were enriched
1420 in progeny ("P") and mature ("M") cell state subclusters. In epidermal and intestinal lineages,
1421 X2/PIWI-LOW ("P-LO") signature transcripts were most highly enriched in neoblast/transition
1422 state and progeny subclusters. In the protonephridial lineage X2/PIWI-LO transcripts were more
1423 uniformly distributed, possibly due to fewer subclusters (and/or lower resolution of transition
1424 states) in this scRNA-Seq dataset.
1425

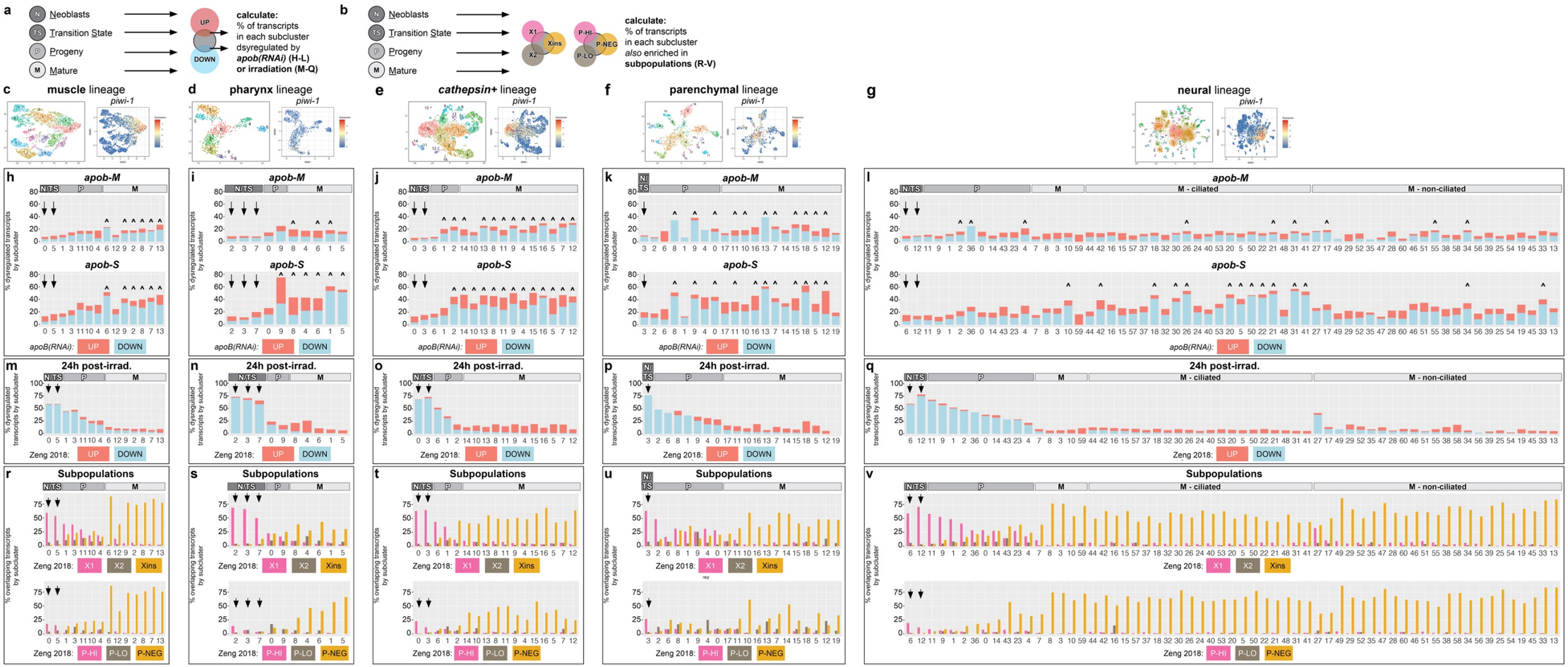

Supplementary Figure 8.

1429 **Supplementary Figure 8. Additional examples of dysregulation of transcripts in**
1430 **differentiating neoblast progeny and mature cells by *apob* RNAi. (a)** Generic scheme used
1431 to identify overlap of transcripts enriched in specific subclusters/cell states[40] that were
1432 dysregulated in *apob(RNAi)* planarians (this study) or 24 hr post-irradiation[49]. **(b)** Generic
1433 scheme to calculate proportion of cell-state-enriched transcripts[40] also enriched in sorted
1434 planarian cell subpopulations[49]. **(c-g)** t-SNE plots (digiworm.wi.mit.edu) indicate subclusters and
1435 *piwi-1* mRNA expression for each lineage. **(h-l)** *apob* knockdown dysregulated greater
1436 proportions of transcripts in progeny ("P") and mature ("M") subclusters in multiple cell type
1437 lineages. Arrows indicate less-affected transcripts in neoblast/transition state ("N/TS")
1438 subclusters. **(m-q)** Cross-referencing of scRNA-Seq data[40] with RNA-Seq data from whole
1439 planarians 24 hr post-irradiation[49]. Transcripts enriched in neoblasts/transition state subclusters
1440 were preferentially downregulated 24 hr post-irradiation (arrows), by contrast to the effects of
1441 *apob* RNAi (H-L). **(r-v)** Cross-referencing of scRNA-Seq data[40] with bulk sorted cell RNA-Seq
1442 data[49]. Histograms showing that X1/PIWI-HI ("P-HI") signature transcripts were primarily
1443 enriched in neoblast ("N"), transition state ("TS"), and progeny ("P) subclusters; that X2/PIWI-
1444 LOW ("P-LO") signature transcripts were most highly enriched in progeny subclusters; and that
1445 Xins/PIWI-NEG ("P-NEG") signature transcripts were enriched in mature ("M") cell state
1446 subclusters. Carets (^) indicate significant gene expression overlap (**h-l**, $p<0.05$, Fisher's exact
1447 test, see Source Data 2 for individual *p* values).
1448

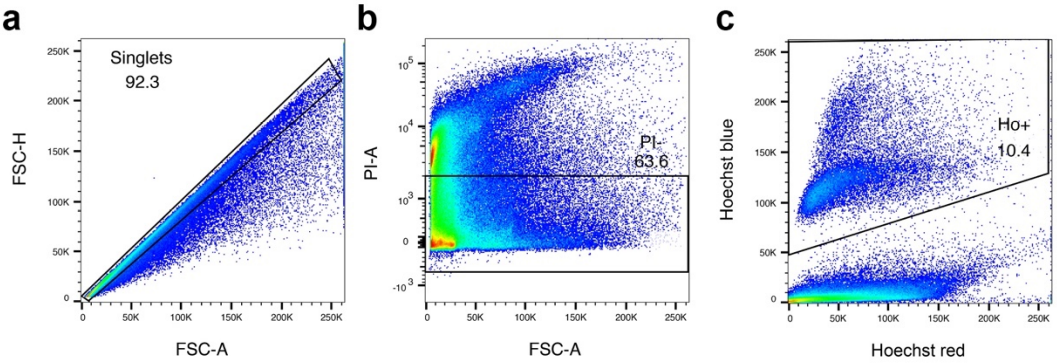

1449

1450

1451 **Supplementary Figure 9.**

1452 **Supplementary Figure 9. Gating strategy for flow cytometry experiments. (a)** Forward
1453 scatter height (FSC-H) vs. forward scatter area (FSC-A) gate to limit to singlet events. **(b)**
1454 Propidium iodide (PI-A) vs. forward scatter area (FSC-A) gate to limit to PI negative (e.g., non-
1455 dead) events. **(c)** Hoechst 33342 blue (y-axis) vs. Hoechst 33342 red (x-axis) gates to limit to
1456 Hoechst-positive (e.g., ≥2C DNA content) events. Percentages of events after each gating step
1457 are indicated.
1458

1459 ## Supplementary Data

1460

1461 **Supplementary Data 1. Up- and downregulated transcripts in *nkx2.2(RNAi)* planarians. (a)**
1462 RNA-Seq data for all transcripts detected in uninjured control vs. *nkx2.2(RNAi)* planarians,
1463 together with best BLAST hits for human/mouse/zebrafish/fly/*C. elegans*. **(b)** RNA-Seq data for
1464 766 significantly downregulated transcripts in *nkx2.2(RNAi)* relative to control planarians. **(c)**
1465 RNA-Seq data for 719 significantly upregulated transcripts in *nkx2.2(RNAi)* relative to control
1466 planarians.

1467

1468 **Supplementary Data 2. Gene Ontology Biological Process terms enriched for transcripts**
1469 **up- and downregulated by *nkx2.2* RNAi. (a)** Biological Process term enrichment data for 766
1470 transcripts downregulated in *nkx2.2(RNAi)* planarians. **(b)** Biological Process term enrichment
1471 data for 719 transcripts upregulated in *nkx2.2(RNAi)* planarians.

1472

1473 **Supplementary Data 3. Transcripts annotated with lipid-related Gene Ontology terms in**
1474 **whole fragment planarian regeneration transcriptome. (a)** Transcripts annotated with the
1475 term "lipid transport." **(b)** Transcripts annotated with the term "triglyceride." **(c)** Transcripts
1476 annotated with the term "cholesterol." Expression data are derived from NCBI GEO GSE107874
1477 [49] mapped to the dd_Smed_v6 transcriptome [105] (see Methods). Some transcripts may be
1478 annotated with multiple GO terms sharing the key words indicated, and therefore have multiple
1479 entries.

1480

1481 **Supplementary Data 4. Up- and downregulated transcripts in *apob(RNAi)* "mild" and**
1482 **"severe" planarians. (a)** RNA-Seq data for all transcripts detected in uninjured control vs.
1483 *apob-1(RNAi);apob-2(RNAi)* planarians, together with best BLAST hits for

1484 human/mouse/zebrafish/fly/*C. elegans*. **(b)** RNA-Seq data for 842 significantly upregulated
1485 transcripts in *apob-M(RNAi)* relative to control planarians. **(c)** RNA-Seq data for 1960
1486 significantly upregulated transcripts in *apob-S(RNAi)* relative to control planarians. **(d)** RNA-Seq
1487 data for 1139 significantly downregulated transcripts in *apob-M(RNAi)* relative to control
1488 planarians. **(e)** RNA-Seq data for 2547 significantly downregulated transcripts in *apob-S(RNAi)*
1489 relative to control planarians.
1490
1491 **Supplementary Data 5. Gene Ontology Biological Process terms enriched for transcripts**
1492 **up- and downregulated by *apob* RNAi. (a)** Biological Process term enrichment data for 842
1493 transcripts upregulated in *apob-M(RNAi)* planarians. **(b)** Biological Process term enrichment
1494 data for 1960 transcripts upregulated in *apob-S(RNAi)* planarians. **(c)** Biological Process term
1495 enrichment data for 1139 transcripts downregulated in *apob-M(RNAi)* planarians. **(d)** Biological
1496 Process term enrichment data for 2547 transcripts downregulated in *apob-S(RNAi)* planarians.
1497
1498 **Supplementary Data 6. Gene and transcript identities used in phylogenetic analyses and**
1499 **gene expression studies. (a)** ApoB and related homologs used for domain diagram and
1500 phylogenetic analysis. **(b)** Alignment of N-terminal Vitellogenin domains used for phylogenetic
1501 tree. **(c)** Lipoprotein receptor homologs used for domain diagram. **(d)** Transcript identities,
1502 sequences, cloning primers and vectors used in this study.
1503
1504 **Source Data 1. Differential expression analysis of neoblast subpopulations from**
1505 **GSE107874.**
1506
1507 **Source Data 2. Numerical data and statistical analyses.**